
Omni-Dimensional Frequency Learner for General Time Series Analysis

Xianing Chen¹ Hanting Chen¹ Hailin Hu¹

Abstract

Frequency domain representation of time series feature offers a concise representation for handling real-world time series data with inherent complexity and dynamic nature. However, current frequency-based methods with complex operations still fall short of state-of-the-art time domain methods for general time series analysis. In this work, we present Omni-Dimensional Frequency Learner (ODFL) model based on a in depth analysis among all the three aspects of the spectrum feature: channel redundancy property among the frequency dimension, the sparse and un-salient frequency energy distribution among the frequency dimension, and the semantic diversity among the variable dimension. Technically, our method is composed of a semantic-adaptive global filter with attention to the un-salient frequency bands and partial operation among the channel dimension. Empirical results show that ODFL achieves consistent state-of-the-art in five mainstream time series analysis tasks, including short- and long-term forecasting, imputation, classification, and anomaly detection, offering a promising foundation for time series analysis.

1. Introduction

Time series analysis, including the tasks of long/short-term forecasting (Lim & Zohren, 2021; Spyros Makridakis, 2018), imputation (Friedman, 1962), anomaly detection (Xu et al., 2021), and classification (Bagnall et al., 2018), has immense practical value in real-world applications such as energy, finance, signal processing (Taylor et al., 2018). Thus, it is crucial to design a general-purpose model for different tasks (Wu et al., 2023) other than focus on specific task in previous works (Woo et al., 2022). However, it is challenging to model time series with inherent complexity and dynamic nature, especially for its sparse, mixing, and overlapped multiple variations (Zhou et al., 2022b; Wu et al., 2023).

Fortunately, the frequency domain representation of time series data offers a more concise representation of its intricate information. It is much easier to model the intrinsic properties of time-series data, e.g. cyclic, trend, global interaction. Thus, FEDFormer (Zhou et al., 2022b) enhances feature extracted from transformer-based model by incorporating spectral information. TimesNet (Wu et al., 2023) extract multi-periodicity feature by segmenting data based on frequencies. However, their proposed complex operations which focus on designing extra sophisticated structures to work with the traditional architecture makes them heavy-weight. Moreover, they still cannot achieve better performance to the state-of-the-art time domain methods (Nie et al., 2022).

This raise the questions of constructing frequency domain time series model: *how to extract frequency domain feature gracefully? And how to extract the most informative part among the frequency domain feature?*

We start with a global filter (Gu et al., 2022) as our baseline operator whose kernel size is equal to the sequence length after transforming latent representation into the frequency domain via Fourier transform, as shown in Figure 1(a). The operator can efficiently modeling global and cyclic information through the simple element-wise multiplication which mathematically equals to circular global convolution that can be served as a global token mixer (Wei et al., 2022) in the origin latent space (McGille & Cooper, 1984) with only $\mathcal{O}(N \log N)$ complexity. Although this operator is able to handle the complex long-range arena (LRA) sequence (Tay et al., 2020), language (Li et al., 2022) and image (Rao et al., 2021) data, it fall short of the state-of-the-art methods for time series analysis (Zhou et al., 2022a). The reason behind can be explained by lacking key properties for time series spectrum feature which should be introduced to the designation of the global kernel.

Consider a time series data $\mathbb{R}^{m \times L}$ with m variates and length L . We can project it to a frequency domain feature $\mathbb{C}^{m \times C \times N}$ under the channel independent setting (Nie et al., 2022) via Fourier transform, where C is the channel number, $N = \lfloor \frac{L}{2} + 1 \rfloor$ is the frequency length. As a result, there are three dimensions to consider for modeling the time series spectrum feature, i.e. the variable dimension, the channel dimension, the frequency dimension. We will detailed the

¹Huawei Noah’s Ark Lab.

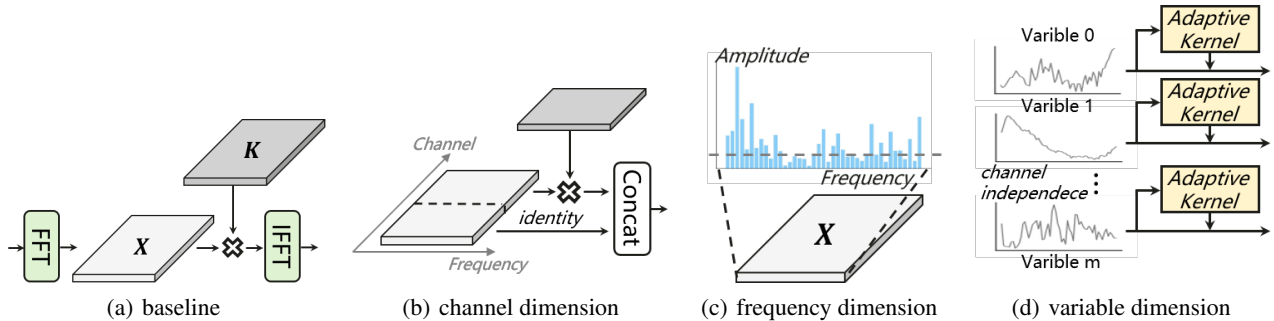


Figure 1. Illustration of (a) the baseline operator, (b) the partial operation, (c) the unsalient frequency bands feature extraction, (d) the semantic diversity and adaptation under the channel independent setting.

insight of our design follow the three perspectives as shown in Figure 1.

The first one is the channel redundancy property among the channel dimension, i.e. the feature map in the frequency domain shares high similarities among different channels as shown in Figure 2, where we randomly visualize a sequence with input length 720 on the latent frequency space on ETTh1 dataset. Although this redundant information often guarantees a comprehensive understanding of the input data which cannot be directly removed (Han et al., 2019; Nie et al., 2021), the collapsed feature still affects the expressive power significantly (Wang et al., 2023c). To make full use of the channel redundancy property as well as increasing channel-wise feature diversity, we propose a simple yet effective partial operation which apply the global filter on only a part of the input channels for frequency feature extraction and leaves the remaining channels untouched as illustrated in Figure 1(b).

Secondly we analyze the frequency dimension. Similar to images (Ruderman, 1994; Riad et al., 2022), sounds (Singh & Theunissen, 2003), and surfaces (Kuroki et al., 2018), energy of time series signals is highly distributed in the lower frequencies. However, time series energy distributed in the higher parts plays a key role as discussed in (Wu et al., 2023), which reflects important trends (Zhou et al., 2022b). Inspired by the sparse kernel (Dai et al., 2022) for extracting the most informative elements, we let the kernel operate on the salient frequency parts only as shown in Figure 1(c), while leaving other low signal-to-noise ratio (SNR) parts unchanged which are still informative even less important. In this way, the model can preserve critical historical information while avoiding overfitting to noise.

Thirdly, the adaptability to semantics also matters under the channel independence setting (Nie et al., 2022; Zeng et al., 2023) among the variable dimension. The feature extractor should be variable semantic adaptive not only instance-aware (Vaswani et al., 2017; Xiao et al., 2022) as shown in

Figure 1(d). For example, the Traffic dataset in the forecasting task has 862 independent variable dimensions. Besides, the spectrum feature is not translation equivariance (Craig, 1985) which requires the operator to be spatial-specific and can adaptively allocate the weights over different frequency bands. Thus, instead of using a static filter, we adopt a simple linear layer to learn semantic adaptive filter from the frequency representations. Then we calculate the element-wise multiplication between the learned filter and the spectrum feature.

Empowering by above key insights, our proposed module can dynamically extract the most informative parts among the frequency domain gracefully. Then we transform the filtered latent feature back into the original time domain space via inverse Fourier transform and process it with Feed-forward network (FFN) follow the modern architecture design (Wang et al., 2023a; Liu et al., 2022b).

With the above module as the primary operator, we build our model named as Omni-Dimensional Frequency Learner (ODFL). Empirically, ODFL improves the baseline global kernel significantly as well as achieves the consistent state-of-the-art on five mainstream time series analysis tasks, which demonstrate our consistent superiority and the excellent task-generalization ability.

2. Related Work

Many task-specific methods are proposed recently, including the Transformer- (Xu et al., 2021; Choromanski et al., 2020; Zhou et al., 2021; Li et al., 2019; Wu et al., 2021; Liu et al., 2022a), MLP- (Phba et al., 2021; Zhang et al., 2022a; Oreshkin et al., 2019; Challu et al., 2022), CNN-based (Wang et al., 2023b; Liu et al., 2021; Borovykh et al., 2017; Bai et al., 2018; He & Zhao, 2019), and classical (Chen & Guestrin, 2016; Taylor et al., 2018; Berndt & Clifford, 1994; Rasheed & Alhadjj, 2014; Vlachos et al., 2005) methods. These methods have learned the dependen-

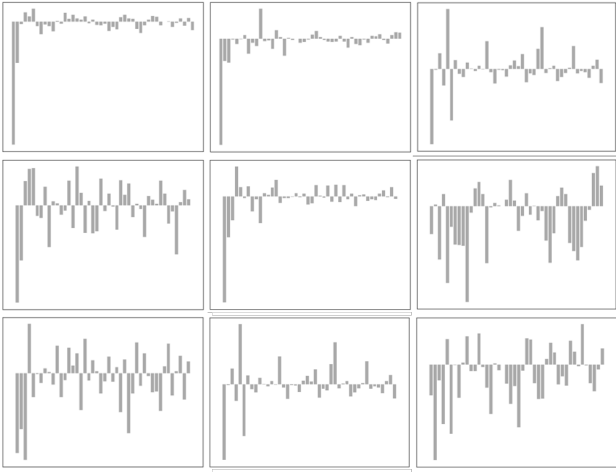


Figure 2. Visualization of channel redundancy in the frequency domain. Only the real part is visualized. Qualitatively, we can see the high redundancies across different channels.

cies in the time domain. For instance, MICN (Wang et al., 2023b) proposes a multi-scale convolution structure to combine local features and global correlations in time series. PatchTST (Nie et al., 2022) propose channel-independent learning and patching design for time series forecasting and shows superior performance than linear model (Zeng et al., 2023). SCINet (Liu et al., 2021) introduces a recursive downsample-convolve-interact architecture to model time series with complex temporal dynamics. Besides, DLinear (Zeng et al., 2023) proposes a set of simple one-layer linear model to learn temporal relationships between input and output sequences.

Several recent works try to enhance time series feature in the frequency domain for time series forecasting. For example, FEDFormer (Zhou et al., 2022b) enhances the seasonal-trend decomposition by using self-attention within the frequency domain. S4 (Gu et al., 2022; Li et al., 2022) comes up with recursive memory design for data representation on Long Range Arena. SFM (Zhang et al., 2017) decomposes the hidden state of LSTM into frequencies. StemGNN (Cao et al., 2020) performs graph convolutions based on Graph Fourier Transform (GFT) and computes series correlations based on Discrete Fourier Transform. AutoFormer (Wu et al., 2021) replaces self-attention by proposing the auto-correlation mechanism implemented with Fast Fourier Transform. FreTS (Yi et al., 2023) propose to directly apply MLPs in the frequency domain to capture global and periodic patterns. FiLM (Zhou et al., 2022a) applies Legendre Polynomials projections to approximate historical information and uses Fourier projection to remove noise. However, they still fail to serve as a general-purpose model for diverse tasks as well as achieve better performance than traditional

time domain methods. We propose a new architecture in the frequency domain that consider the key properties among the variable, channel, frequency dimensions thus can be generalized to various time series task.

To achieve task-general ability, TimesNet (Wu et al., 2023) proposes to transform the 1D time-series data into 2D space based on multiple periods to model intraperiod- and interperiod-variations, but it neglects a lot of valuable information in the frequency domain and is heavy-weight. OFA (Zhou et al., 2023) explores to use large scale pre-trained frozen language models to serve as an universal compute engine (Lu et al., 2022; Giannou et al., 2023) to leverage inductive biases learned from language data (Radford et al., 2019) instead of introducing inductive biases by architecture designation. Also, Lag-Llama (Rasul et al., 2023) investigate the use of pre-trained time series models from Monash dataset (Godahewa et al., 2021) for zero-shot forecasting. Our work takes a step further to enhance the line of deep models and frequency domain feature modeling by introducing general inductive biases to fully leverage the property the time series feature in both time and frequency domain.

3. Method

3.1. Preliminaries: Discrete Fourier Transform

Given a sequence of time series data $x[n], 0 \leq n \leq N - 1$, Discrete Fourier Transform (DFT) converts the sequence into the frequency domain by:

$$X[k] = \sum_{n=0}^{N-1} x[n] e^{-j(2\pi/N)kn}, 0 \leq k \leq N - 1. \quad (1)$$

where j is the imaginary unit. $X[k]$ represents the spectrum of the sequence $x[n]$ at the frequency $\omega_k = \frac{2\pi k}{N}$. Conversely, we can recover the original sequence by the inverse DFT (IDFT) given the $X[k]$:

$$x[n] = \frac{1}{N} \sum_{k=0}^{N-1} X[k] e^{j(2\pi/N)kn}. \quad (2)$$

For real input $x[n]$, DFT is conjugate symmetric, i.e., $X[N - k] = X^*[k]$ (see Appendix B.1). Thus, we can only keep half of the DFT $\{X[k] : 0 \leq k \leq \lceil \frac{N}{2} \rceil\}$ to save memory and computation costs. To compute the DFT, the Fast Fourier Transform (FFT) is widely used which reduces the complexity of DFT from $\mathcal{O}(N^2)$ to $\mathcal{O}(N \log N)$. Inverse fast Fourier transform (IFFT) can also be used for computing IDFT, which is similar to FFT.

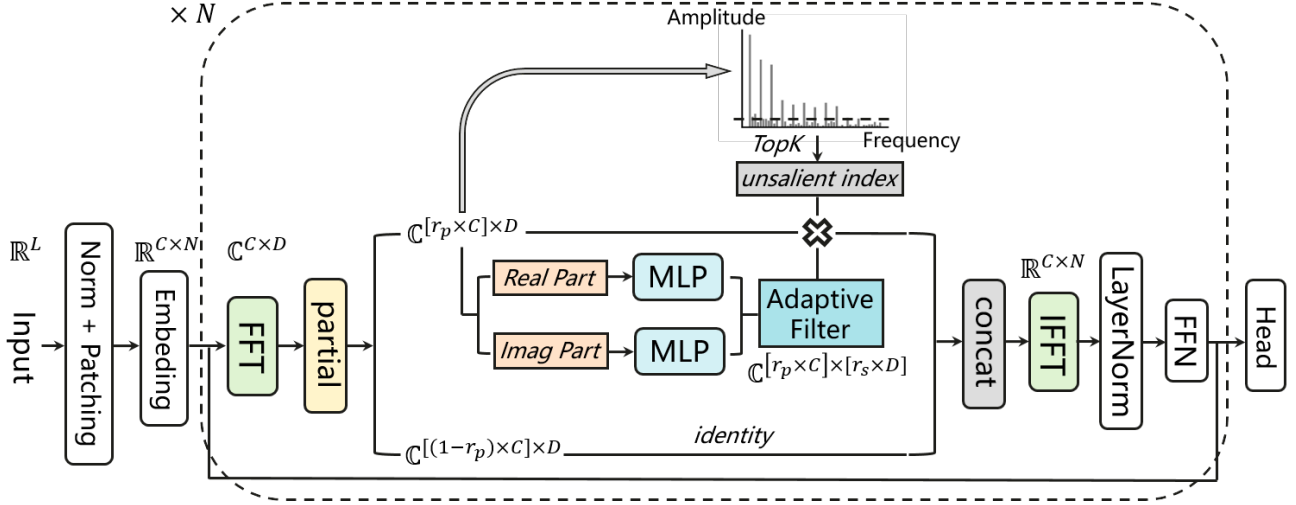


Figure 3. The architecture of our proposed method. The transformed frequency feature is firstly partial to two parts. Then, our learned adaptive filter is applied on only a few inputs channels and the unsalient frequency bands while leaving the remaining ones untouched. For simplicity, we only take one variable example for visualization.

3.2. Frequency Learner Architecture

Overall Structure. The overall architecture we employ is depicted in Figure 3. Given the length L input time series data $\mathbf{x} \in \mathbb{R}^{m \times L}$ with m variates normalized by ReVIN instance normalization (Kim et al., 2022), we follow (Nie et al., 2022) to split \mathbf{x} to m univariate series $\mathbf{x}^{(i)} \in \mathbb{R}^{1 \times L}$, $i = 1, \dots, m$, where each of them is fed independently into the ODFL model. Each input univariate series $\mathbf{x}^{(i)}$ is divided into patches with patch length P and stride S and generate a sequence $\mathbf{x}_p^{(i)} \in \mathbb{R}^{P \times N}$ where $N = \lfloor \frac{L-P}{S} \rfloor + 2$ is the patches number. Then the sequence is project to a sequence feature $\mathbf{x}^{(i)} \in \mathbb{R}^{C \times N}$ by a linear layer. Finally, the feature is fed into our ODFL blocks and corresponding head to obtain the final output.

Baseline. We start with a simple global filter to process the feature $\mathbf{x} \in \mathbb{R}^{C \times N}$ as our baseline, index i is omit for simplicity. We firstly transform \mathbf{x} into the frequency domain via FFT. Since \mathbf{x} is a real tensor, the frequency domain feature is conjugate symmetric. Thus, we can only take half of the values but preserve the complete information (Appendix B.1) and get the complex frequency domain feature $\mathbf{X} \in \mathbb{C}^{C \times D}$, where $D = \lfloor \frac{N}{2} + 1 \rfloor$ is the frequency length. Then we extract feature by element-wise multiplying a learnable filter:

$$\widetilde{\mathbf{X}} = \mathbf{X} \odot \mathbf{K}. \quad (3)$$

where $\mathbf{K} \in \mathbb{C}^{C \times D}$. The equation is equivalent to the global circular convolution with global kernel in the time domain which can serve as a global token mixer (Appendix B.2).

Extract Feature on Partial Channels. While the redundant features (Han et al., 2019) in $\mathbf{X} \in \mathbb{C}^{C \times D}$ provide a wealth of information, they decrease the diversity of the filter as well as increasing computation costs.

To takes advantage of the redundancy, we apply the filter on only a part of the spectrum feature channels while leaving the remaining ones untouched:

$$\widetilde{\mathbf{X}}_{1:[r_p \times D]} = \mathbf{X}_{1:[r_p \times D]} \odot \mathbf{K}. \quad (4)$$

where r_p is the partial ratio (PR), $\mathbf{K} \in \mathbb{C}^{[r_p \times C] \times D}$.

We calculate the effective dimension ratio $r_{d(\epsilon)}$ follow the analysis method from (Cai et al., 2021). The effective dimension $d(\epsilon)$ is defined as the minimum principal component numbers that occupy the explained variance ratio of ϵ in a principal component analysis (PCA), and the effective dimension ratio $r_{d(\epsilon)}$ is the proportion to dimension number. Thus, a more powerful representation of a feature among the channel dimension would result in a larger effective dimension ratio and vice versa.

The smaller ratio of the baseline model in Figure 4 shows the feature collapse problem. It can be observed that adding the partial operation increase the effective dimension to the great extent, indicating the significant role of our proposed components in channel-wise feature diversity, by separating the latent feature into two parts and transforming the processed one into another feature space.

Extract Feature in Un-Salient Parts. Consider the sparsity (Wu et al., 2023) and noisy (Chatfield, 1980) in the

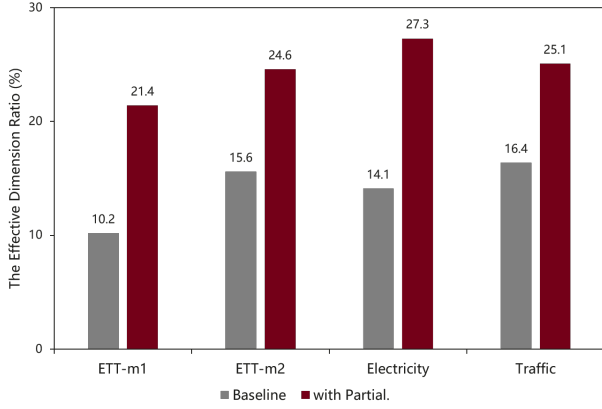


Figure 4. The effective dimension ratio $r_{d(0.8)}$ of our model which reflects the feature redundant and diversity. Higher effective dimension ratio indicates more diverse feature among channel dimension.

frequency domain, we take a step further to consider the salient spectrum parts only which can serve as the low-rank approximation for fourier basis (Zhou et al., 2022b). We first get the amplitude of each frequency which represents its importance as shown in the upper part in Figure 3:

$$\mathbf{A} = \text{Avg}(\text{Amp}(\mathbf{X})). \quad (5)$$

where $\text{Amp}(\cdot)$ denote the calculation of amplitude values. $\mathbf{A} \in \mathbb{R}^D$ represents the calculated amplitude of each frequency, which is averaged from C dimensions by $\text{Avg}(\cdot)$. Then we select the tok-k amplitude frequencies as the salient frequencies:

$$\{f_1, \dots, f_k\} = \arg \text{Topk}(\mathbf{A})_{f_* \in \{1, \dots, D\}} \quad (6)$$

where k is a hyper-parameter, $k \leq D$, and $f_1 < \dots < f_k$. We denote $r_s = \frac{k}{D}$ as the sparsity ratio (SR). Afterward, we can extract features from the salient bands by multiplying our learnable sparse kernel:

$$\widetilde{\mathbf{X}}_{1:[r_p \times D]}[f_1, \dots, f_k] = \mathbf{X}_{1:[r_p \times D]}[f_1, \dots, f_k] \odot \mathbf{K}. \quad (7)$$

where $\mathbf{K} \in \mathbb{C}^{[r_p \times C] \times [r_s \times D]}$. Here for other un-salient frequencies $f \notin \{f_1, \dots, f_k\}$, we simply keep them unchanged in $\widetilde{\mathbf{X}}$ since these low SNR parts still have valuable information when transforming back into the time domain, and dropping them (i.e. setting the values to zero) will cause the Picket Fence Effect (Li & Chen, 2008).

Learn Semantic-Adaptive Filter Among the Variable Dimension. The adaptability to semantics has played the

key role in feature modeling (Wei et al., 2022; Jie et al., 2019) instead of passively determining by manual designed rules (Tolstikhin et al., 2021) especially under the channel independence setting. With the expectation for our operator as semantic-adaptive, the weights \mathbf{K} should be adaptive to \mathbf{X} . We utilize simply linear layer by separately considering the real and imaginary mappings to learn the adaptive filter motivated by dynamic convolution (Chen et al., 2019). The learned respective real/imaginary parts are then stacked to recover the frequency components in order to obtain the adaptive filter $\mathbf{K} \in \mathbb{C}^{[r_p \times C] \times [r_s \times D]}$ in Equation (7).

Output. The feature is transform back into the original time domain by using IFFT algorithm. Then, LayerNorm (Ba et al., 2016) and inverted FFN layer (Sandler et al., 2018) is applied to fully leverage the information from all channels. We stack multiple proposed blocks for constructing our Frequency Learner model. Finally, the output time domain feature from the last module is passed to corresponding head according to different tasks.

4. Experiments

In this section, we evaluate the performance of our proposed method on five mainstream tasks, including short- and long-term forecasting, imputation, classification and anomaly detection to verify its generality. Then, we provide an ablation study for the impact of each choice and analyze the model properties.

4.1. Benchmarks.

The summary of benchmarks adhered to the experimental settings of TimesNet (Wu et al., 2023) are list in Table 1. Follow OFA (Zhou et al., 2023) and PatchTST (Nie et al., 2022), Exchange dataset is not contained for the long-term forecasting task, since (Zeng et al., 2023) shows that simply repeating the last value in the look-back window can outperform or be comparable to the best results.

4.2. Baselines.

We choose the latest and advanced time series model as our basic baselines, including Transformer-based models: OFA (Zhou et al., 2023), PatchTST (Nie et al., 2022), FEDFormer (Zhou et al., 2022b), CrossFormer (Zhang & Yan, 2023), ETSFormer (Woo et al., 2022); MLP-based models: Dlinear (Zeng et al., 2023), LightTS (Zhang et al., 2022a), FreTS (Yi et al., 2023); and convolution-based models: TimesNet (Wu et al., 2023), SCINet (Liu et al., 2021), MICN (Wang et al., 2023b). Besides, N-HiTS (Challu et al., 2022) and N-BEATS (Oreshkin et al., 2019) are used for short-term forecasting. Anomaly Transformer (Xu et al., 2021) is used for anomaly detection. XGBoost (Chen & Guestrin, 2016), Rocket (Dempster et al., 2020), LSTNet (Lai et al., 2018),

Table 1. Summary of experiment benchmarks. See detailed benchmark description in Appendix A.1.

Tasks	Benchmarks	Metrics	Series Length
Forecasting	Long-term: ETT (4 subsets), Electricity, Traffic, Weather, ILI	MSE, MAE	96~720 (ILI: 24~60)
	Short-term: M4 (6 subsets)	SMAPE, MASE, OWA	6~48
Imputation	ETT (4 subsets), Electricity, Weather	MSE, MAE	96
Classification	UEA (10 subsets)	Accuracy	29~1751
Anomaly Detection	SMD, MSL, SMAP, SWaT, PSM	Precision, Recall, F1-Socre	100

Table 2. Long-term forecasting task. All the results are averaged from 4 different prediction lengths, that is {24, 36, 48, 60} for ILI and {96, 192, 336, 720} for the others. See Table 18 in Appendix G for the full results. The best and second best results are in **Bold** and underline.

Models	ODFL (Ours)	TimesNet (2023)	PatchTST (2023)	Cross. (2023)	DLinear (2023)	FED. (2022)	MICN (2023)	SCINet (2022)	ETS. (2022)	OFA (2023)	LightTS (2022)	FreTS (2023)
Metric	MSE MAE	MSE MAE	MSE MAE	MSE MAE	MSE MAE	MSE MAE	MSE MAE	MSE MAE	MSE MAE	MSE MAE	MSE MAE	MSE MAE
ETTm1	0.343 <u>0.378</u>	0.400 0.406	<u>0.351</u> 0.381	0.431 0.443	0.357 <u>0.379</u>	0.382 0.422	0.383 0.406	0.387 0.411	0.429 0.425	0.352 0.383	0.435 0.437	0.362 0.386
ETTm2	0.246 <u>0.313</u>	0.291 0.333	<u>0.255</u> <u>0.315</u>	0.632 0.578	0.267 0.332	0.292 0.343	0.277 0.336	0.294 0.355	0.293 0.342	0.266 0.326	0.409 0.436	0.274 0.335
ETTth1	0.413 <u>0.432</u>	0.458 0.450	0.413 <u>0.432</u>	0.441 0.465	0.423 0.437	0.428 0.454	0.433 0.462	0.460 0.462	0.542 0.510	0.427 0.426	0.491 0.479	0.426 0.448
ETTth2	<u>0.331</u> <u>0.384</u>	0.414 0.427	0.330 0.380	0.835 0.676	0.431 0.447	0.388 0.434	0.385 0.430	0.371 0.410	0.439 0.452	0.346 0.394	0.602 0.543	0.413 0.435
Electricity	0.158 <u>0.253</u>	0.192 0.295	<u>0.161</u> 0.252	0.278 0.339	0.177 0.274	0.207 0.321	0.182 0.292	0.191 0.277	0.208 0.323	0.167 0.263	0.229 0.329	0.164 0.264
Traffic	0.388 <u>0.265</u>	0.620 0.336	<u>0.390</u> 0.263	0.513 0.290	0.434 0.295	0.604 0.372	0.525 0.312	0.577 0.376	0.621 0.396	0.414 0.294	0.622 0.392	0.423 0.292
Weather	0.221 <u>0.260</u>	0.259 0.287	<u>0.225</u> <u>0.264</u>	0.230 0.290	0.240 0.300	0.310 0.357	0.242 0.298	0.287 0.317	0.271 0.334	0.237 0.270	0.261 0.312	0.232 0.276
ILI	1.431 0.792	2.139 0.931	<u>1.443</u> <u>0.797</u>	3.361 1.235	2.160 1.041	2.597 1.070	2.567 1.055	2.253 1.021	2.497 1.004	1.925 0.903	7.382 2.003	1.976 0.972

S4 (Gu et al., 2022) are used for classification.

Besides, we implement a strong baseline for the baseline operator in Equation (3), which equipped with the channel independent setting that converts the multivariate data into univariate data and patch design from (Nie et al., 2022) to avoid under-estimating the results of baseline which have achieved comparable performance to the state-of-the-art methods as described below.

4.3. Main Results.

Our proposed method achieves consistent state-of-the-art performance on five mainstream tasks. We provide the detailed results of each task below.

Long- and Short-term Forecasting. We adopt two types of benchmarks, including long-term and short-term forecasting, to evaluate the forecasting performance. For the long-term setting, we follow the benchmarks used in OFA (Zhou et al., 2023) and PatchTST (Nie et al., 2022), including ETT (Zhou et al., 2021), Electricity (UCI), Traffic (PeMS), Weather (Wetterstation), and ILI (CDC), covering five real-world applications. For the short-term setting, we adopt the

M4 (Spyros Makridakis, 2018) dataset, which contains the yearly, quarterly, monthly collected univariate marketing data and so on. As shown in Table 2, 3, our ODFL shows great performance in both long- and short-term settings.

Imputation. We use the datasets from the electricity and weather scenarios as our benchmarks, including ETT (Zhou et al., 2021), Electricity (UCI) and Weather (Wetterstation), where the data-missing problem happens commonly. To compare the model capacity under different proportions of missing data, we randomly mask the time points in the ratio of {12.5%, 25%, 37.5%, 50%}. As shown in Table 4, our ODFL surpasses the prior SOTA on all benchmarks with a large margin.

Classification. Follow the benchmark proposed by TimesNet (Wu et al., 2023), we use 10 multivariate sequence-level classification datasets from UEA Time Series Classification Archive (Bagnall et al., 2018), covering the gesture, action and audio recognition, medical diagnosis by heart-beat monitoring and other practical tasks to verify the model performance on high-level tasks. As shown in Figure 5, our ODFL achieves SOTA with an average accuracy of 74.1%.

Table 3. Short-term forecasting task on M4. The prediction lengths are in [6, 48], and results are weighted averaged from several datasets under different sample intervals. See Table 19 in Appendix G for full results.

Models	ODFL (Ours)	TimesNet (2023)	PatchTST (2023)	Cross. (2023)	DLinear (2023)	FED. (2022)	MICN (2023)	SCINet (2022)	ETS. (2022)	OFA (2023)	LightTS (2022)	Station.N-HiTSN (2022)	BEATS (2019)	FreTS (2023)
SMape	11.734	11.829	12.059	13.474	13.639	12.840	13.130	12.396	14.718	11.991	13.525	12.780	11.927	11.851
MASE	1.576	1.585	1.623	1.866	2.095	1.701	1.896	1.677	2.408	1.600	2.111	1.756	1.613	1.599
OWA	0.845	0.851	0.869	0.985	1.051	0.918	0.980	0.894	1.172	0.861	1.051	0.930	0.861	0.855

Table 4. Imputation task. We randomly mask {12.5%, 25%, 37.5%, 50%} time points in length-96 time series. The results are averaged from 4 different mask ratios. See Table 20 in Appendix G for full results.

Models	ODFL (Ours)	TimesNet (2023)	PatchTST (2023)	Cross. (2023)	DLinear (2023)	FED. (2022)	MICN (2023)	SCINet (2022)	ETS. (2022)	OFA (2023)	LightTS (2022)	FreTS (2023)
Metric	MSE MAE	MSE MAE	MSE MAE	MSE MAE	MSE MAE	MSE MAE	MSE MAE	MSE MAE	MSE MAE	MSE MAE	MSE MAE	MSE MAE
ETTh1	0.0160.087	0.0270.107	0.0450.133	0.0410.143	0.0930.206	0.0620.177	0.0700.182	0.0390.129	0.1200.253	0.0280.105	0.1040.218	0.0360.105
ETTh2	0.0180.083	0.0220.088	0.0280.098	0.0460.149	0.0960.208	0.1010.215	0.1440.249	0.0270.102	0.2080.327	0.0210.084	0.0460.151	0.0300.104
ETTh1	0.0480.148	0.0780.187	0.1330.236	0.1320.251	0.2010.306	0.1170.246	0.1250.250	0.1040.216	0.2020.329	0.0690.173	0.2840.373	0.0970.210
ETTh2	0.0380.125	0.0490.146	0.0660.164	0.1220.240	0.1420.259	0.1630.279	0.2050.307	0.0640.165	0.3670.436	0.0480.141	0.1190.250	0.0670.166
Electricity	0.0790.195	0.0920.210	0.0910.209	0.0830.199	0.1320.260	0.1300.259	0.1190.247	0.0860.201	0.2140.339	0.0900.207	0.1310.262	0.0990.218
Weather	0.0250.047	0.0300.054	0.0330.057	0.0360.050	0.0520.110	0.0990.203	0.0560.128	0.0310.053	0.0760.171	0.0310.056	0.0550.117	0.0490.112

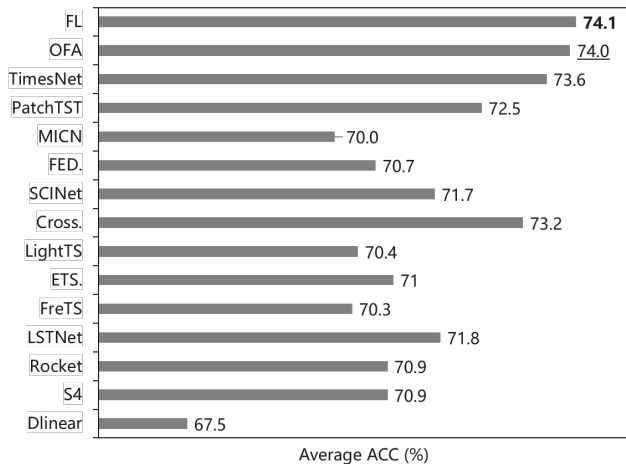


Figure 5. Model comparison in classification. The results are averaged from 10 subsets of UEA. Higher accuracy indicates better performance. See Table 22 in Appendix G for full results.

Anomaly Detection. We compare models on five widely-used anomaly detection benchmarks: SMD (Su et al., 2019), MSL (Hundman et al., 2018), SMAP (Hundman et al., 2018), SWaT (Mathur & Tippenhauer, 2016), PSM (Abdulaal et al., 2021), covering service monitoring, space & earth exploration, and water treatment applications. Following the pre-processing methods in Anomaly Transformer (Xu et al., 2021), we split the dataset into consecutive non-overlapping segments by sliding window. As shown in Figure 6, our

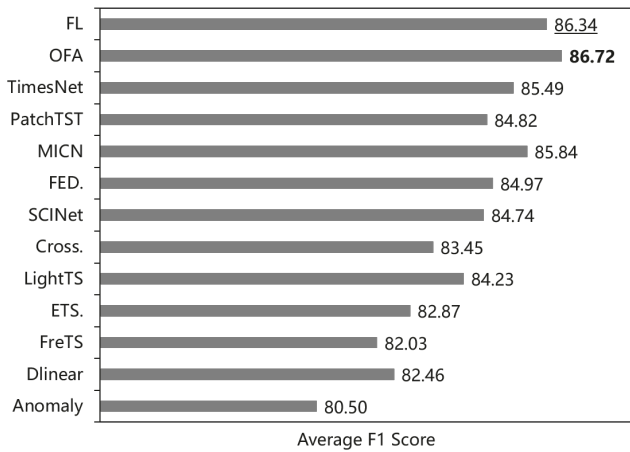


Figure 6. Model comparison in anomaly detection tasks. The results are averaged from several datasets. Higher F1 score indicates better performance. See Table 21 in Appendix G for full results.

ODFL also achieves SOTA performance, this demonstrates that our model satisfies the property that each task requires with high generalization ability.

4.4. Ablation Study

Ablation of the Block Design. To validate the effectiveness of our designation within the proposed ODFL block, we ablate the important elements of our design on long-term forecasting task. Results are shown on Table 5. As we can

Table 5. Ablation of different modules evaluated on long-term forecasting task. The symbol + means indicates that we add the corresponding element upon the upper line.

Dataset	ETTM1		ETTM2		ETTh1		ETTh2		Electricity		Traffic		Weather		ILI	
Metric	MSE	MAE	MSE	MAE	MSE	MAE	MSE	MAE	MSE	MAE	MSE	MAE	MSE	MAE	MSE	MAE
Baseline	0.372	0.403	0.274	0.336	0.431	0.453	0.382	0.430	0.188	0.277	0.428	0.299	0.235	0.270	1.927	0.913
+ <i>Partial.</i>	0.360	0.393	0.259	0.328	0.424	0.445	0.356	0.401	0.179	0.270	0.413	0.283	0.231	0.277	1.769	0.914
+ <i>Salient.</i>	0.354	0.389	0.255	0.320	0.421	0.440	0.343	0.391	0.170	0.263	0.404	0.277	0.225	0.265	1.636	0.853
+ <i>Adaptive.</i>	0.343	0.378	0.246	0.313	0.413	0.432	0.331	0.384	0.158	0.253	0.388	0.265	0.221	0.260	1.431	0.792

Table 6. Ablation of the partial ratio on long-term forecasting task. A higher ratio means more channels are extracted.

Dataset	ETTM1		ETTM2		ETTh1		ETTh2		Electricity		Traffic		Weather		ILI	
r_p	MSE	MAE	MSE	MAE	MSE	MAE	MSE	MAE	MSE	MAE	MSE	MAE	MSE	MAE	MSE	MAE
100%	0.355	0.391	0.258	0.322	0.420	0.437	0.346	0.393	0.163	0.258	0.396	0.269	0.227	0.266	1.625	0.843
75%	0.349	0.385	0.250	0.314	<u>0.415</u>	0.431	<u>0.335</u>	0.383	0.159	0.255	0.391	<u>0.267</u>	0.222	0.264	1.547	0.819
50%	0.343	0.378	0.246	0.313	0.413	<u>0.432</u>	0.331	0.384	<u>0.158</u>	<u>0.253</u>	0.388	0.265	0.221	0.260	1.431	0.792
25%	0.346	0.379	<u>0.247</u>	0.313	0.416	0.435	0.338	0.388	0.156	0.252	0.389	<u>0.267</u>	0.221	<u>0.263</u>	1.511	0.813

see in the first line, the baseline with the global filter described above has inferior performance compared with self attention in the time domain (Nie et al., 2022) similar to the phenomena observed in (Zhou et al., 2022a). After adding our partial operation on the channel dimension, the model can outperform the baseline model with fewer parameters as shown in the second line. To better incorporate with time series properties, we introduce the sparsity operation on the salient frequency parts which improves the model performance by extracting the most informative elements while avoiding overfitting to the low SNR parts as shown in the third line. Finally, thanks to our semantic-aware adaptive filter, the performance increases consistently by handing the varied semantics as shown in the last line which represents our proposed ODFL model.

Varying Partial Ratio. To verify the impact of the partial ratio r_p in Equation (4), we conduct ablation experiments on long-term forecasting task in Table 6, which empirically shows that the partial operation can improve performance when vary in a wide range consistently. The result verifies the previous statement. As a result, for the partial ratio r_p , we set it to 50% for all variants by default for both effectiveness and efficiency.

Varying Sparsity Ratio. We conduct a brief ablation study on the value of sparsity ratio r_s in Equation (7), results are summarized in Table 7. A too large sparsity ratio r_s would make the kernel degrade to a regular global filter which will be affected by the noisy frequency bands, while

a too small value would render our filter less effective in capturing the spectrum features. Thus, we simply set r_s to 75% by default for simplicity. Besides, we compare other frequency modes selection strategy in Appendix C.1.

4.5. Model Analysis

Compared with SGConv Module. SGConv (Li et al., 2022) propose two basic principles for the global kernel network S4 (Gu et al., 2022) with a special parameterization based on the Cauchy kernel: the number of parameters should scale sub-linearly with sequence length, and the kernel needs to satisfy a decaying structure. This brings performance improvement on the Long Range Arena (LRA) benchmark (Tay et al., 2020). However, this boost is not much on time series tasks as shown in Table 8.

Since simply transferring S4 to time series forecasting task cause much weaker performance than SoTA as shown in (Zhou et al., 2022a), we compare SGConv module under our strong baseline for fair comparison. As shown in the second line on Table 8, replacing the global kernel with SGConv kernel follow the official implementation¹ brings minimal improvement. This is mainly because the LRA task needs more inductive biases for modeling its much long sequence (1K to 16K) and complex data structure. For example, all existing models failed on modeling the spatial-level sequence modeling task Pathfinder-X in the LRA benchmark except S4 which requires sophisticated parameterization

¹<https://github.com/ctlllll/SGConv>.

Table 7. Ablation of the sparsity ratio on long-term forecasting task. A higher ratio means more frequency bands are filtered or extracted.

Dataset	ETTm1		ETTm2		ETTh1		ETTh2		Electricity		Traffic		Weather		ILI	
r_s	MSE	MAE	MSE	MAE	MSE	MAE	MSE	MAE	MSE	MAE	MSE	MAE	MSE	MAE	MSE	MAE
100%	0.350	0.384	0.251	0.317	0.414	0.435	0.341	0.390	0.166	0.261	0.395	0.268	0.225	0.263	1.501	0.808
75%	0.343	0.378	0.246	0.313	0.413	0.432	0.331	0.384	0.158	0.253	0.388	0.265	0.221	0.260	1.431	0.792
50%	0.344	0.380	0.250	0.314	0.415	0.436	0.333	0.387	0.161	0.255	0.389	0.267	0.223	0.261	1.463	0.795

Table 8. Comparison results of SGConv module. The symbol + means indicates that we add the corresponding element upon the baseline.

Dataset	ETTm1		ETTm2		ETTh1		ETTh2		Electricity		Traffic		Weather		ILI	
Metric	MSE	MAE	MSE	MAE	MSE	MAE	MSE	MAE	MSE	MAE	MSE	MAE	MSE	MAE	MSE	MAE
Baseline	0.372	0.403	0.274	0.336	0.431	0.453	0.382	0.430	0.188	0.277	0.428	0.299	0.235	0.270	1.927	0.913
+SGConv.	0.368	0.400	0.269	0.334	0.432	0.450	0.380	0.433	0.180	0.276	0.430	0.301	0.230	0.270	1.905	0.903
ODFL	0.343	0.378	0.246	0.313	0.413	0.432	0.331	0.384	0.158	0.253	0.388	0.265	0.221	0.260	1.431	0.792

and initialization schemes that combine the wisdom from several prior works. Also, the exponential decay property of the spectrum of matrix powers for time series signal is much easier to learn from our semantic-aware kernel and un-salient frequency selection strategy as visualized in Appendix F. Moreover, we find that different from other field, the initialization of the kernel shows minimal impact for time series task as detailed in Appendix C.4.

Compared with TimesNet. TimesNet (Wu et al., 2023) also demonstrates excellent generality in time series analysis tasks as well as taking advantage of frequency representation by capturing unsalient period-variation. However, they accomplish this goal by transforming the 1D time series into 2D space and model the cyclic information by 2D convolution operation. This additional transformation and aggregation operation makes TimesNet heavy-weight and hard to train. Moreover, it can model limited significant frequencies only and will neglect valuable information within the frequency domain. On the contrary, as described in Appendix B.3, our proposed ODFL can model every significant frequency simply by multiplication operation.

Benefiting from Representation Learning. Sophisticated deep models with larger capacity than linear (Zeng et al., 2023) or classical statistical (Hyndman et al., 2008) models that capture abstract representation of the data can benefiting from self-supervised learning techniques (Nie et al., 2022; Eldele et al., 2021; Yang & Linda Qiao, 2022; Zhang et al., 2022b). In this part, we follow the masked self-supervised learning method (He et al., 2021) and setting that we randomly remove a portion of input sequence and then the model is trained to recover the missing contents from PatchTST (Nie et al., 2022) on all the long-term forecasting

training datasets. After that we fine-tune the pre-trained model on the corresponding dataset. The result in Table 9 show that ODFL can be further enhanced by representation learning.

Table 9. The results of representation learning.

Models		Fine-tuning		Supervised	
Metric		MSE	MAE	MSE	MAE
ETTm1	96	0.280	0.341	0.282	0.343
	192	0.319	0.365	0.322	0.368
	336	0.355	0.385	0.356	0.388
	720	0.405	0.401	0.412	0.411
Weather	96	0.140	0.195	0.145	0.198
	192	0.184	0.230	0.190	0.238
	336	0.236	0.275	0.240	0.279
	720	0.300	0.318	0.309	0.330
Electricity	96	0.126	0.221	0.128	0.224
	192	0.144	0.240	0.145	0.240
	336	0.160	0.256	0.162	0.260
	720	0.190	0.281	0.195	0.288
Traffic	96	0.358	0.390	0.369	0.402
	192	0.401	0.412	0.409	0.425
	336	0.418	0.430	0.425	0.441
	720	0.442	0.451	0.449	0.461

5. Conclusion

In this work, we proposes the Frequency Learner as a task-general model for time series analysis. We propose three key feature properties for modeling time series feature in the frequency domain: channel redundancy, sparse frequency dis-

tribution, and semantic diversity. By utilizing our semantic-aware global filter with sparse operation along both the channel and frequency dimension, ODFL achieves state-of-the-art performance on five mainstream tasks.

In the future work, we will further explore the large-scale self-supervised pre-training methods upon our proposed ODFL model to achieve better task-general ability.

References

- Abdulaal, A., Liu, Z., and Lancewicki, T. Practical approach to asynchronous multivariate time series anomaly detection and localization. *KDD*, 2021.
- Ba, J. L., Kiros, J. R., and Hinton, G. E. Layer normalization. 2016.
- Bagnall, A. J., Dau, H. A., Lines, J., Flynn, M., Large, J., Bostrom, A. G., Southam, P., and Keogh, E. J. The uea multivariate time series classification archive, 2018. *arXiv preprint arXiv:1811.00075*, 2018.
- Bai, S., Kolter, J. Z., and Koltun, V. An empirical evaluation of generic convolutional and recurrent networks for sequence modeling. *arXiv preprint arXiv:1803.01271*, 2018.
- Berndt, D. J. and Clifford, J. Using dynamic time warping to find patterns in time series. In *KDD Workshop*, 1994.
- Borovykh, A., Bohte, S., and Oosterlee, C. W. Conditional time series forecasting with convolutional neural networks. *arXiv preprint arXiv:1703.04691*, 2017.
- Cai, X., Huang, J., Bian, Y.-L., and Church, K. W. Isotropy in the contextual embedding space: Clusters and manifolds. In *International Conference on Learning Representations*, 2021. URL <https://api.semanticscholar.org/CorpusID:235614342>.
- Cao, D., Wang, Y., Duan, J., Zhang, C., Zhu, X., Huang, C., Tong, Y., Xu, B., Bai, J., Tong, J., and Zhang, Q. Spectral temporal graph neural network for multivariate time-series forecasting. *ArXiv*, abs/2103.07719, 2020. URL <https://api.semanticscholar.org/CorpusID:227276243>.
- CDC. Illness. <https://gis.cdc.gov/grasp/fluview/fluportaldashboard.html>.
- Challu, C., Olivares, K. G., Oreshkin, B. N., Garza, F., Mergenthaler, M., and Dubrawski, A. N-hits: Neural hierarchical interpolation for time series forecasting. *arXiv preprint arXiv:2201.12886*, 2022.
- Chatfield, C. *The analysis of time series:an introduction*. The analysis of time series:an introduction, 1980.
- Chen, T. and Guestrin, C. Xgboost: A scalable tree boosting system. *KDD*, 2016.
- Chen, Y., Dai, X., Liu, M., Chen, D., Yuan, L., and Liu, Z. Dynamic convolution: Attention over convolution kernels. *2020 IEEE/CVF Conference on Computer Vision and Pattern Recognition (CVPR)*, pp. 11027–11036, 2019. URL <https://api.semanticscholar.org/CorpusID:208910380>.
- Choromanski, K., Likhoshesterov, V., Dohan, D., Song, X., Gane, A., Sarlos, T., Hawkins, P., Davis, J., Mohiuddin, A., Kaiser, L., et al. Rethinking attention with performers. *arXiv preprint arXiv:2009.14794*, 2020.
- Craig. A review of time-domain and frequency-domain component mode synthesis method. 1985.
- Dai, X., Li, M., Zhai, P., Tong, S., Gao, X., Huang, S.-L., Zhu, Z., You, C., and Ma, Y. Revisiting sparse convolutional model for visual recognition. *arXiv preprint arXiv:2210.12945*, 2022.
- Dempster, A., Petitjean, F., and Webb, G. I. Rocket: exceptionally fast and accurate time series classification using random convolutional kernels. *Data Min. Knowl. Discov.*, 2020.
- Eldele, E., Ragab, M., Chen, Z., Wu, M., Kwoh, C., Li, X., and Guan, C. Time-series representation learning via temporal and contextual contrasting. In *International Joint Conference on Artificial Intelligence*, 2021. URL <https://api.semanticscholar.org/CorpusID:235658361>.
- Friedman, M. The interpolation of time series by related series. *J. Amer. Statist. Assoc.*, 1962.
- Giannou, A., Rajput, S., yong Sohn, J., Lee, K., Lee, J. D., and Papailiopoulos, D. Looped transformers as programmable computers. *ArXiv*, abs/2301.13196, 2023. URL <https://api.semanticscholar.org/CorpusID:256389656>.
- Godahewa, R., Bergmeir, C., Webb, G. I., Hyndman, R. J., and Montero-Manso, P. Monash time series forecasting archive. *ArXiv*, abs/2105.06643, 2021. URL <https://api.semanticscholar.org/CorpusID:234681550>.
- Gu, A., Goel, K., and Ré, C. Efficiently modeling long sequences with structured state spaces. In *ICLR*, 2022.
- Han, K., Wang, Y., Tian, Q., Guo, J., Xu, C., and Xu, C. Ghostnet: More features from cheap operations. *2020 IEEE/CVF Conference on Computer Vision and Pattern Recognition (CVPR)*, pp. 1577–1586, 2019. URL <https://api.semanticscholar.org/CorpusID:208310058>.

- He, K., Chen, X., Xie, S., Li, Y., Doll'ar, P., and Girshick, R. B. Masked autoencoders are scalable vision learners. *2022 IEEE/CVF Conference on Computer Vision and Pattern Recognition (CVPR)*, pp. 15979–15988, 2021. URL <https://api.semanticscholar.org/CorpusID:243985980>.
- He, Y. and Zhao, J. Temporal convolutional networks for anomaly detection in time series. *J. Phys. Conf. Ser.*, 2019.
- Hundman, K., Constantinou, V., Laporte, C., Colwell, I., and Söderström, T. Detecting spacecraft anomalies using lstms and nonparametric dynamic thresholding. *KDD*, 2018.
- Hyndman, R., Koehler, A. B., Ord, J. K., and Snyder, R. D. *Forecasting with exponential smoothing: the state space approach*. Springer Science & Business Media, 2008.
- Jie, Shen, Samuel, Albanie, Gang, Sun, and Enhua. Squeeze-and-excitation networks. *IEEE transactions on pattern analysis and machine intelligence*, 2019.
- Kim, T., Kim, J., Tae, Y., Park, C., Choi, J., and Choo, J. Reversible instance normalization for accurate time-series forecasting against distribution shift. In *International Conference on Learning Representations*, 2022. URL <https://api.semanticscholar.org/CorpusID:251647808>.
- Kingma, D. and Ba, J. Adam: A method for stochastic optimization. *Computer Science*, 2014.
- Kuroki, S., Sawayama, M., and Nishida, S. Haptic texture perception on 3d-printed surfaces transcribed from visual natural textures. In *EuroHaptics*, 2018. URL <https://api.semanticscholar.org/CorpusID:46949970>.
- Lai, G., Chang, W.-C., Yang, Y., and Liu, H. Modeling long-and short-term temporal patterns with deep neural networks. In *SIGIR*, 2018.
- Li, S., Jin, X., Xuan, Y., Zhou, X., Chen, W., Wang, Y.-X., and Yan, X. Enhancing the locality and breaking the memory bottleneck of transformer on time series forecasting. In *NeurIPS*, 2019.
- Li, Y., Cai, T., Zhang, Y., huai Chen, D., and Dey, D. What makes convolutional models great on long sequence modeling? *ArXiv*, abs/2210.09298, 2022. URL <https://api.semanticscholar.org/CorpusID:252917984>.
- Li, Y. F. and Chen, K. F. Eliminating the picket fence effect of the fast fourier transform. *Computer Physics Communications*, 178(7):486–491, 2008.
- Lim, B. and Zohren, S. Time-series forecasting with deep learning: a survey. *Philos. Trans. Royal Soc. A*, 2021.
- Liu, M., Zeng, A., Chen, M.-H., Xu, Z., Lai, Q., Ma, L., and Xu, Q. Scinet: Time series modeling and forecasting with sample convolution and interaction. In *Neural Information Processing Systems*, 2021. URL <https://api.semanticscholar.org/CorpusID:252873681>.
- Liu, Y., Wu, H., Wang, J., and Long, M. Non-stationary transformers: Rethinking the stationarity in time series forecasting. In *NeurIPS*, 2022a.
- Liu, Z., Mao, H., Wu, C., Feichtenhofer, C., Darrell, T., and Xie, S. A convnet for the 2020s. *2022 IEEE/CVF Conference on Computer Vision and Pattern Recognition (CVPR)*, pp. 11966–11976, 2022b. URL <https://api.semanticscholar.org/CorpusID:245837420>.
- Lu, K., Grover, A., Abbeel, P., and Mordatch, I. Frozen pretrained transformers as universal computation engines. In *AAAI Conference on Artificial Intelligence*, 2022. URL <https://api.semanticscholar.org/CorpusID:250301249>.
- Mathur, A. P. and Tippenhauer, N. O. Swat: a water treatment testbed for research and training on ICS security. In *CySWATER*, 2016.
- McGillem, C. D. and Cooper, G. R. Continuous and discrete signal and system analysis. 1984. URL <https://api.semanticscholar.org/CorpusID:117907785>.
- Musbah, H., Mo, E. H., and Aly, H. Identifying seasonality in time series by applying fast fourier transform. In *2019 IEEE Electrical Power and Energy Conference (EPEC)*, 2019.
- Nie, Y., Han, K., Liu, Z., Xiao, A., Deng, Y., Xu, C., and Wang, Y. Ghostsr: Learning ghost features for efficient image super-resolution. *Trans. Mach. Learn. Res.*, 2022, 2021. URL <https://api.semanticscholar.org/CorpusID:231662136>.
- Nie, Y., Nguyen, N. H., Sinthong, P., and Kalagnanam, J. A time series is worth 64 words: Long-term forecasting with transformers. *arXiv preprint arXiv:2211.14730*, 2022.
- Oreshkin, B. N., Carpov, D., Chapados, N., and Bengio, Y. N-BEATS: Neural basis expansion analysis for interpretable time series forecasting. *ICLR*, 2019.
- Paszke, A., Gross, S., Massa, F., Lerer, A., Bradbury, J., Chanan, G., Killeen, T., Lin, Z., Gimelshein, N., Antiga,

- L., Desmaison, A., Köpf, A., Yang, E., DeVito, Z., Raison, M., Tejani, A., Chilamkurthy, S., Steiner, B., Fang, L., Bai, J., and Chintala, S. Pytorch: An imperative style, high-performance deep learning library. In *NeurIPS*, 2019.
- PeMS. Traffic. <http://pems.dot.ca.gov/>.
- Phba, B., Oz, A., and Jpt, A. A covid-19 time series forecasting model based on mlp ann. *Procedia Computer Science*, 181:940–947, 2021.
- Radford, A., Wu, J., Child, R., Luan, D., Amodei, D., and Sutskever, I. Language models are unsupervised multitask learners. 2019. URL <https://api.semanticscholar.org/CorpusID:160025533>.
- Rao, Y., Zhao, W., Zhu, Z., Lu, J., and Zearlyhou, J. Global filter networks for image classification. In *Advances in Neural Information Processing Systems (NeurIPS)*, 2021.
- Rasheed, F. and Alhaji, R. A framework for periodic outlier pattern detection in time-series sequences. *IEEE Trans Cybern*, 2014.
- Rasul, K., Ashok, A., Williams, A. R., Khorasani, A., Adamopoulos, G., Bhagwatkar, R., Bilovs, M., Ghonia, H., Hassen, N., Schneider, A., Garg, S., Drouin, A., Chapados, N., Nevmyvaka, Y., and Rish, I. Lag-llama: Towards foundation models for time series forecasting. *ArXiv*, abs/2310.08278, 2023. URL <https://api.semanticscholar.org/CorpusID:263909560>.
- Riad, R., Teboul, O., Grangier, D., and Zeghidour, N. Learning strides in convolutional neural networks. *ICLR*, 2022.
- Ruderman, D. L. The statistics of natural images. *Network: Computation In Neural Systems*, 5:517–548, 1994. URL <https://api.semanticscholar.org/CorpusID:2793971>.
- Sandler, M., Howard, A. G., Zhu, M., Zhmoginov, A., and Chen, L.-C. Mobilenetv2: Inverted residuals and linear bottlenecks. *2018 IEEE/CVF Conference on Computer Vision and Pattern Recognition*, pp. 4510–4520, 2018. URL <https://api.semanticscholar.org/CorpusID:4555207>.
- Singh, N. C. and Theunissen, F. E. Modulation spectra of natural sounds and ethological theories of auditory processing. *The Journal of the Acoustical Society of America*, 114 6 Pt 1:3394–411, 2003. URL <https://api.semanticscholar.org/CorpusID:24226567>.
- Spyros Makridakis. M4 dataset, 2018. URL <https://github.com/M4Competition/M4-methods/tree/master/Dataset>.
- Su, Y., Zhao, Y., Niu, C., Liu, R., Sun, W., and Pei, D. Robust anomaly detection for multivariate time series through stochastic recurrent neural network. *KDD*, 2019.
- Tay, Y., Dehghani, M., Abnar, S., Shen, Y., Bahri, D., Pham, P., Rao, J., Yang, L., Ruder, S., and Metzler, D. Long range arena: A benchmark for efficient transformers. *ArXiv*, abs/2011.04006, 2020. URL <https://api.semanticscholar.org/CorpusID:260440449>.
- Taylor, Sean, J., Letham, and Benjamin. Forecasting at scale. *American Statistician*, 2018.
- THUML. Time-series-library, 2023. URL <https://github.com/thuml/Time-Series-Library>.
- Tolstikhin, I. O., Houlsby, N., Kolesnikov, A., Beyer, L., Zhai, X., Unterthiner, T., Yung, J., Keysers, D., Uszkoreit, J., Lucic, M., and Dosovitskiy, A. Mlp-mixer: An all-mlp architecture for vision. In *Neural Information Processing Systems*, 2021. URL <https://api.semanticscholar.org/CorpusID:233714958>.
- UCI. Electricity. <https://archive.ics.uci.edu/ml/datasets/ElectricityLoadDiagrams20112014>.
- Vaswani, A., Shazeer, N., Parmar, N., Uszkoreit, J., Jones, L., Gomez, A. N., Kaiser, L., and Polosukhin, I. Attention is all you need. In *NeurIPS*, 2017.
- Vlachos, M., Yu, P. S., and Castelli, V. On periodicity detection and structural periodic similarity. In *SDM*, 2005.
- Wang, A., Chen, H., Lin, Z., Pu, H., and Ding, G. Repvit: Revisiting mobile cnn from vit perspective. *ArXiv*, abs/2307.09283, 2023a. URL <https://api.semanticscholar.org/CorpusID:259951457>.
- Wang, H., Peng, J., Huang, F., Wang, J., Chen, J., and Xiao, Y. Micn: Multi-scale local and global context modeling for long-term series forecasting. In *International Conference on Learning Representations*, 2023b. URL <https://api.semanticscholar.org/CorpusID:259298592>.
- Wang, Y., Chen, H., Tang, Y., Guo, T., Han, K., Nie, Y., Wang, X., Hu, H., Bai, Z., Wang, Y., Liu, F., Liu, Z., Guo, J., Zeng, S., Zhang, Y., Xu, Q., Liu, Q., Yao, J., Xu, C., and Tao, D. Pangu- π : Enhancing language model architectures via nonlinearity compensation. 2023c. URL <https://api.semanticscholar.org/CorpusID:266690973>.

- Wei, G., Zhang, Z., Lan, C., Lu, Y., and Chen, Z. Active token mixer. In *AAAI Conference on Artificial Intelligence*, 2022. URL <https://api.semanticscholar.org/CorpusID:255096211>.
- Wetterstation. Weather. <https://www.bgc-jena.mpg.de/wetter/>.
- Woo, G., Liu, C., Sahoo, D., Kumar, A., and Hoi, S. C. H. Etsformer: Exponential smoothing transformers for time-series forecasting. *arXiv preprint arXiv:2202.01381*, 2022.
- Wu, H., Xu, J., Wang, J., and Long, M. Autoformer: Decomposition transformers with Auto-Correlation for long-term series forecasting. In *NeurIPS*, 2021.
- Wu, H., Hu, T., Liu, Y., Zhou, H., Wang, J., and Long, M. Timesnet: Temporal 2d-variation modeling for general time series analysis. In *International Conference on Learning Representations*, 2023.
- Xiao, Q., Wu, B., Zhang, Y., Liu, S., Pechenizkiy, M., Mocanu, E., and Mocanu, D. C. Dynamic sparse network for time series classification: Learning what to "see". *ArXiv*, abs/2212.09840, 2022. URL <https://api.semanticscholar.org/CorpusID:254103020>.
- Xu, J., Wu, H., Wang, J., and Long, M. Anomaly transformer: Time series anomaly detection with association discrepancy. In *ICLR*, 2021.
- Yang, L. and Linda Qiao. Unsupervised time-series representation learning with iterative bilinear temporal-spectral fusion. In *International Conference on Machine Learning*, 2022. URL <https://api.semanticscholar.org/CorpusID:246706116>.
- Yi, K., Zhang, Q., Fan, W., Wang, S., Wang, P., He, H., Lian, D., An, N., Cao, L., and Niu, Z. Frequency-domain mlps are more effective learners in time series forecasting. *ArXiv*, abs/2311.06184, 2023. URL <https://api.semanticscholar.org/CorpusID:265128791>.
- Zeng, A., Chen, M., Zhang, L., and Xu, Q. Are transformers effective for time series forecasting? 2023.
- Zhang, L., Aggarwal, C. C., and Qi, G.-J. Stock price prediction via discovering multi-frequency trading patterns. *Proceedings of the 23rd ACM SIGKDD International Conference on Knowledge Discovery and Data Mining*, 2017. URL <https://api.semanticscholar.org/CorpusID:28307599>.
- Zhang, T., Zhang, Y., Cao, W., Bian, J., Yi, X., Zheng, S., and Li, J. Less is more: Fast multivariate time series forecasting with light sampling-oriented mlp structures. *arXiv preprint arXiv:2207.01186*, 2022a.
- Zhang, X., Zhao, Z., Tsiligkaridis, T., and Zitnik, M. Self-supervised contrastive pre-training for time series via time-frequency consistency. *ArXiv*, abs/2206.08496, 2022b. URL <https://api.semanticscholar.org/CorpusID:249848167>.
- Zhang, Y. and Yan, J. Crossformer: Transformer utilizing cross-dimension dependency for multivariate time series forecasting. In *International Conference on Learning Representations*, 2023. URL <https://api.semanticscholar.org/CorpusID:259298223>.
- Zhou, H., Zhang, S., Peng, J., Zhang, S., Li, J., Xiong, H., and Zhang, W. Informer: Beyond efficient transformer for long sequence time-series forecasting. In *AAAI*, 2021.
- Zhou, T., Ma, Z., Wang, X., Wen, Q., Sun, L., Yao, T., and Jin, R. Film: Frequency improved legendre memory model for long-term time series forecasting. *ArXiv*, abs/2205.08897, 2022a. URL <https://api.semanticscholar.org/CorpusID:248863240>.
- Zhou, T., Ma, Z., Wen, Q., Wang, X., Sun, L., and Jin, R. FEDformer: Frequency enhanced decomposed transformer for long-term series forecasting. In *ICML*, 2022b.
- Zhou, T., Niu, P., Wang, X., Sun, L., and Jin, R. One fits all: Power general time series analysis by pretrained lm. *arXiv preprint arXiv:2302.11939*, 2023.

A. Setting

A.1. Benchmark

We provide the detailed dataset descriptions in Table 10.

We adopt the mean square error (MSE) and mean absolute error (MAE) for long-term forecasting and imputations. For anomaly detection, we adopt the F1-score as the metric. For the short-term forecasting, we adopt the symmetric mean absolute percentage error (SMAPE), mean absolute scaled error (MASE) and overall weighted average (OWA) as the metrics:

$$\text{SMAPE} = \frac{200}{H} \sum_{i=1}^H \frac{|\mathbf{X}_i - \widehat{\mathbf{X}}_i|}{|\mathbf{X}_i| + |\widehat{\mathbf{X}}_i|}, \quad (8)$$

$$\text{MAPE} = \frac{100}{H} \sum_{i=1}^H \frac{|\mathbf{X}_i - \widehat{\mathbf{X}}_i|}{|\mathbf{X}_i|}, \quad (9)$$

$$\text{MASE} = \frac{1}{H} \sum_{i=1}^H \frac{|\mathbf{X}_i - \widehat{\mathbf{X}}_i|}{\frac{1}{H-m} \sum_{j=m+1}^H |\mathbf{X}_j - \mathbf{X}_{j-m}|}, \quad (10)$$

$$\text{OWA} = \frac{1}{2} \left[\frac{\text{SMAPE}}{\text{SMAPE}_{\text{Naive2}}} + \frac{\text{MASE}}{\text{MASE}_{\text{Naive2}}} \right]. \quad (11)$$

where m is the periodicity of the data. $\mathbf{X}, \widehat{\mathbf{X}} \in \mathbb{R}^{H \times C}$ are the ground truth and prediction results of the future with H time points and C dimensions. \mathbf{X}_i means the i -th future time point.

A.2. Implementation Details

All experiments are implemented in PyTorch 1.10.0² (Paszke et al., 2019) and conducted on a single NVIDIA V100 32GB GPU. All the experiments are repeated 3 times with different seeds and the means of the metrics are reported as the final results. Our implementation is built on the Time Series Library framework (THUML, 2023). The linear head with a flatten layer is used to obtain the final prediction. We use patch length $P = 16$ and stride $S = 8$ for all experiments follow (Nie et al., 2022) except that for short-term forecasting task with very short sequence we simply set patch length $P = 1$ and stride $S = 1$. Follow (Wu et al., 2023), we select the d_{model} based on the input series dimension C by $\min\{\max\{2^{\lceil \log C \rceil}, d_{\text{min}}\}, d_{\text{max}}\}$ to handle various dimensions of input sequence. The partial ratio is set to 50% and the sparsity ratio is set to 75%. The FFN ratio is set to 4. We use the Adam (Kingma & Ba, 2014) optimizer with (β_1, β_2) as (0.9, 0.999). The initial learning rate is listed in Table 11. Learning rate is dropped by half every epoch. An early stopping counter is employed to stop the training process after ten epochs if no loss degradation on the valid set is observed.

We collect some baseline results from OFA (Zhou et al., 2023) and re-run other baselines under the same setting in (Wu et al., 2023) follow the official implementation, where all the baselines are re-run with various hyper-parameters and the best results are chosen to avoid under-estimating the baselines.

Besides, for the long-term forecasting task we also re-run them with vary input length $L \in \{24, 48, 96, 192, 336, 512, 720\}$ follow (Zhou et al., 2023; Nie et al., 2022) and choose the best results. Moreover, we re-run FreTS (Yi et al., 2023) with ReVIN normalization introduced by its official code³ under the common data loader setting⁴ to have a fair comparison.

²The index operation with complex dtype data for implementing Equation (7) in the lower Pytorch version does not support automatic differentiation.

³<https://github.com/aikunyi/FreTS>.

⁴<https://github.com/youqinie98/PatchTST> and <https://github.com/thuml/Time-Series-Library>.

Omni-Dimensional Frequency Learner for General Time Series Analysis

Table 10. Dataset descriptions. The dataset size is organized in (Train, Validation, Test).

Tasks	Dataset	Dim	Series Length	Dataset Size	Information (Frequency)
Long-term Forecasting	ETTm1, ETTm2	7	{96, 192, 336, 720}	(34465, 11521, 11521)	Electricity (15 mins)
	ETTh1, ETTh2	7	{96, 192, 336, 720}	(8545, 2881, 2881)	Electricity (15 mins)
	Electricity	321	{96, 192, 336, 720}	(18317, 2633, 5261)	Electricity (Hourly)
	Traffic	862	{96, 192, 336, 720}	(12185, 1757, 3509)	Transportation (Hourly)
	Weather	21	{96, 192, 336, 720}	(36792, 5271, 10540)	Weather (10 mins)
	ILI	7	{24, 36, 48, 60}	(617, 74, 170)	Illness (Weekly)
Short-term Forecasting	M4-Yearly	1	6	(23000, 0, 23000)	Demographic
	M4-Quarterly	1	8	(24000, 0, 24000)	Finance
	M4-Monthly	1	18	(48000, 0, 48000)	Industry
	M4-Weakly	1	13	(359, 0, 359)	Macro
	M4-Daily	1	14	(4227, 0, 4227)	Micro
	M4-Hourly	1	48	(414, 0, 414)	Other
Imputation	ETTm1, ETTm2	7	96	(34465, 11521, 11521)	Electricity (15 mins)
	ETTh1, ETTh2	7	96	(8545, 2881, 2881)	Electricity (15 mins)
	Electricity	321	96	(18317, 2633, 5261)	Electricity (15 mins)
	Weather	21	96	(36792, 5271, 10540)	Weather (10 mins)
Classification (UEA)	EthanolConcentration	3	1751	(261, 0, 263)	Alcohol Industry
	FaceDetection	144	62	(5890, 0, 3524)	Face (250Hz)
	Handwriting	3	152	(150, 0, 850)	Handwriting
	Heartbeat	61	405	(204, 0, 205)	Heart Beat
	JapaneseVowels	12	29	(270, 0, 370)	Voice
	PEMS-SF	963	144	(267, 0, 173)	Transportation (Daily)
	SelfRegulationSCP1	6	896	(268, 0, 293)	Health (256Hz)
	SelfRegulationSCP2	7	1152	(200, 0, 180)	Health (256Hz)
	SpokenArabicDigits	13	93	(6599, 0, 2199)	Voice (11025Hz)
UWaveGestureLibrary	3	315	(120, 0, 320)	Gesture	
Anomaly Detection	SMD	38	100	(566724, 141681, 708420)	Server Machine
	MSL	55	100	(44653, 11664, 73729)	Spacecraft
	SMAP	25	100	(108146, 27037, 427617)	Spacecraft
	SWaT	51	100	(396000, 99000, 449919)	Infrastructure
	PSM	25	100	(105984, 26497, 87841)	Server Machine

Table 11. Experiment configuration of our ODFL.

Tasks / Configurations	Model Hyper-parameter			Training Process			
	Layers	d_{\min}^\dagger	d_{\max}^\dagger	LR*	Loss	Batch Size	Epochs
Long-term Forecasting	2	32	512	10^{-4}	MSE	32	100
Short-term Forecasting	2	16	64	10^{-3}	SMAPE	16	100
Imputation	2	64	128	10^{-3}	MSE	16	100
Classification	2	32	64	10^{-3}	Cross Entropy	16	30
Anomaly Detection	3	32	128	10^{-4}	MSE	128	10

$\dagger d_{\text{model}} = \min\{\max\{2^{\lceil \log C \rceil}, d_{\min}\}, d_{\max}\}$, where C is input series dimension.

B. Discussion

B.1. The DFT of real signals are conjugate symmetric

Given a real signal $\mathbf{x} \in \mathbb{R}^n$, the DFT of it $\mathbf{X} \in \mathbb{R}^N$ is conjugate symmetric, which can be proved as follows:

$$\begin{aligned}
 \mathbf{X}[N - k] &= \sum_{n=0}^{N-1} \mathbf{x}[n] e^{-j(2\pi/N)(N-k)n} \\
 &= \sum_{n=0}^{N-1} \mathbf{x}[n] e^{j(2\pi/N)kn} = \mathbf{X}[k].
 \end{aligned} \tag{12}$$

B.2. The filter can serve as a global mixer

We firstly give the definition of circular convolution of a signal $\mathbf{x}[n]$ and a filter $\mathbf{k}[n]$ in the time domain:

$$y[n] = \sum_{m=0}^{N-1} \mathbf{k}[m] \mathbf{x}[(n - m)_N], \tag{13}$$

where $((n))_N$ denotes n modulo N . Then multiplication in the frequency domain with a global kernel $\mathbf{K}[n]$ can be rewritten as follows:

$$\begin{aligned}
 &\mathbf{K}[k] \mathbf{X}[k] \\
 &= \mathbf{K}[k] \sum_{n=0}^{N-1} \mathbf{x}[n] e^{-j(2\pi/N)kn} \\
 &= \mathbf{K}[k] \left(\sum_{n=0}^{N-m-1} \mathbf{x}[n] e^{-j(2\pi/N)kn} + \sum_{n=N-m}^{N-1} \mathbf{x}[n] e^{-j(2\pi/N)kn} \right) \\
 &= \mathbf{K}[k] \left(\sum_{n=m}^{N-1} \mathbf{x}[n - m] e^{-j(2\pi/N)k(n-m)} \right. \\
 &\quad \left. + \sum_{n=0}^{m-1} \mathbf{x}[n - m + N] e^{-j(2\pi/N)k(n-m)} \right) \\
 &= \sum_{m=0}^{N-1} \mathbf{k}[m] e^{-j(2\pi/N)km} \sum_{n=0}^{N-1} \mathbf{x}[(n - m)_N] e^{-j(2\pi/N)k(n-m)} \\
 &= \sum_{n=0}^{N-1} \sum_{m=0}^{N-1} \mathbf{k}[m] \mathbf{x}[(n - m)_N] e^{-j(2\pi/N)kn} \\
 &= Y[k],
 \end{aligned} \tag{14}$$

where $Y[k]$ is the DFT of $y[n]$. Thus, the operation of multiplying our sparse kernel with the salient frequencies $\{f_1, \dots, f_k\}$ is equivalent to multiplying a global kernel $\hat{\mathbf{K}} \in \mathbb{R}^{k \times F}$ with the full frequency feature $\mathbf{X} \in \mathbb{R}^{F \times C}$, where for frequencies $f \notin \{f_1, \dots, f_k\}$, the kernel values are fixed to 1. Thus, our large sparse kernel is also equivalent to a global depth-wise circular convolution in the time domain, which can model global trends.

B.3. ODFL learns seasonality

DFT represents the time series by a set of elementary functions called basis, where each basis $X[k]$ represents the spectrum of the sequence $x[n]$ at the frequency $\omega_k = 2\pi k/N$, which is corresponding to the period length $\lceil \frac{T}{j} \rceil$, as discussed in Equation (1). Thus each element of our kernel \mathbf{K} corresponds to a spectrum of the sequence. Benefiting from this representation, our method can model both long- and short-term seasonality explicitly (Chatfield, 1980; Musbah et al., 2019).

Table 12. Ablation study of the frequency selection strategies.

Dataset	ETTm1		ETTm2		ETTh1		ETTh2		Electricity		Traffic		Weather		ILI	
Metric	MSE	MAE	MSE	MAE	MSE	MAE	MSE	MAE	MSE	MAE	MSE	MAE	MSE	MAE	MSE	MAE
High	0.384	0.411	0.273	0.338	0.436	0.457	0.377	0.413	0.179	0.275	0.419	0.293	0.240	0.278	1.842	0.879
Random	0.355	0.396	0.256	0.321	0.418	0.440	0.337	0.390	0.169	0.262	0.394	0.269	0.225	0.271	1.458	0.799
Low	0.352	0.390	0.258	0.319	0.416	0.437	0.340	0.392	0.165	0.250	0.397	0.273	0.227	0.266	1.491	0.802
Un-salient	0.343	0.378	0.246	0.313	0.413	0.432	0.331	0.384	0.158	0.253	0.388	0.265	0.221	0.260	1.431	0.792

Table 13. Ablation study of the operation for salient part.

Dataset	ETTm1		ETTm2		ETTh1		ETTh2		Electricity		Traffic		Weather		ILI	
Metric	MSE	MAE	MSE	MAE	MSE	MAE	MSE	MAE	MSE	MAE	MSE	MAE	MSE	MAE	MSE	MAE
drop	0.365	0.399	0.271	0.334	0.422	0.439	0.362	0.410	0.169	0.267	0.398	0.272	0.250	0.288	1.477	0.832
keep	0.343	0.378	0.246	0.313	0.413	0.432	0.331	0.384	0.158	0.253	0.388	0.265	0.221	0.260	1.431	0.792

Table 14. Ablation study of the dynamic filter generator.

Dataset	ETTm1		ETTm2		ETTh1		ETTh2		Electricity		Traffic		Weather		ILI	
Metric	MSE	MAE	MSE	MAE	MSE	MAE	MSE	MAE	MSE	MAE	MSE	MAE	MSE	MAE	MSE	MAE
deep	0.342	0.376	0.247	0.313	0.414	0.434	0.330	0.384	0.158	0.253	0.389	0.263	0.222	0.260	1.432	0.795
linear	0.343	0.378	0.246	0.313	0.413	0.432	0.331	0.384	0.158	0.253	0.388	0.265	0.221	0.260	1.431	0.792

C. More Ablation Studies

C.1. Ablation of Frequency Selection Strategies

To prove the effectiveness of our selection strategy, we compare four strategies: our un-salient frequency selection, random selection (Zhou et al., 2022b) which randomly select 40% lowest frequency and 10% highest frequency follow (Zhou et al., 2022a), low-frequency selection (Riad et al., 2022; Zhou et al., 2022a), and high-frequency selection strategies (Zhou et al., 2022a). As shown in Table 12, our salient frequency selection strategy outperforms other methods consistently which shows that although low frequency modes are important, the un-salient modes in the high frequency part still contributes to the time series modeling.

C.2. Ablation Study of the operation for salient part

We keep the salient part unchanged since even though these parts have low SNR, they still contribute to the feature in the time domain at each location. In this section, we verify this by comparing two operations: *keep* and *drop*, where *keep* means

we keep the non-salient parts in the frequency domain unchanged, and *drop* means we set the non-salient parts within the frequency domain to 0. As shown in Table 13, keeping the non-salient parts in the frequency domain still outperforms the *drop* operation, and the *drop* operation continuously decreases the performance; this is mainly because of the Picket Fence Effect of the FFT (Li & Chen, 2008).

C.3. Ablation of the dynamic filter generator

We simply use a linear layer to generate the dynamic kernel which terms *linear* since linear model can already extract trend and periodicity information for time series especially on the embed feature follow (Zeng et al., 2023). In this section, we explore to introduce more non-linearity to the kernel generator which terms *deep*, where the structure of the sub-network is *linear-gelu-linear*. However, the *deep* variant shows limit performance improvement.

Table 15. Effective of kernel parameter initialization.

Dataset	ETTm1		ETTm2		ETTh1		ETTh2		Electricity		Traffic		Weather		ILI	
Metric	MSE	MAE	MSE	MAE	MSE	MAE	MSE	MAE	MSE	MAE	MSE	MAE	MSE	MAE	MSE	MAE
<i>random</i>	0.372	0.403	0.274	0.336	0.431	0.453	0.382	0.430	0.188	0.277	0.428	0.299	0.235	0.270	1.927	0.913
<i>one</i>	0.372	0.403	0.275	0.336	0.432	0.452	0.383	0.430	0.186	0.276	0.429	0.299	0.233	0.270	1.924	0.915
<i>sgconv</i>	0.371	0.402	0.278	0.337	0.431	0.452	0.382	0.430	0.187	0.277	0.428	0.298	0.235	0.270	1.923	0.911

Table 16. The results of noise injection experiment. A $0.1 \times \mathcal{N}(0, 1)$ Gaussian noise is introduced. We conduct four sets of experiments with/without noise in training and test phases. The metric of variants is presented in relative value, where \uparrow indicates degraded performance, and \downarrow indicates improved performance.

Training		w.o. noise		noise	
Testing		w.o. noise	noise	w.o. noise	noise
Long-term Forecasting (MSE)	ETTm1	0.343	$\uparrow 0.29\%$	$\downarrow 0.57\%$	$\uparrow 0.62\%$
	ETTm2	0.246	$\downarrow 0.60\%$	$\downarrow 0.91\%$	$\downarrow 0.09\%$
	ETTh1	0.413	$\downarrow 0.48\%$	$\uparrow 0.11\%$	$\uparrow 0.82\%$
	ETTh2	0.331	$\uparrow 0.24\%$	$\uparrow 0.08\%$	$\downarrow 0.16\%$
Classification (ACC)	EthanolConcentration	36.6	$\downarrow 0.27\%$	$\downarrow 0.82\%$	$\uparrow 0.27\%$
	FaceDetection	69.5	$\downarrow 0.14\%$	$\uparrow 0.36\%$	0.00%
Anomaly Detection (F1 Score)	SMAP	70.44	$\downarrow 0.14\%$	$\uparrow 0.21\%$	$\downarrow 0.04\%$
	MSL	84.43	0.00%	0.00%	0.00%

C.4. Effective of kernel parameter initialization

In Section 4.5, SGConv is compared with our method, the results show that their proposed principles have minimal improvement for time series task which are conflict to the results on the LRA benchmark. To further understand the reason behind the phenomenon in depth, we compare different parameter initialization methods for the global kernel: *random* initialization from normal Gaussian distribution, unified initialization which initialize all parameters to value *one*, and *sgconv* initialization method. The similar results in Table 15 show that the baseline model on time series task is robust to kernel initialization.

D. Noise Injection Experiment

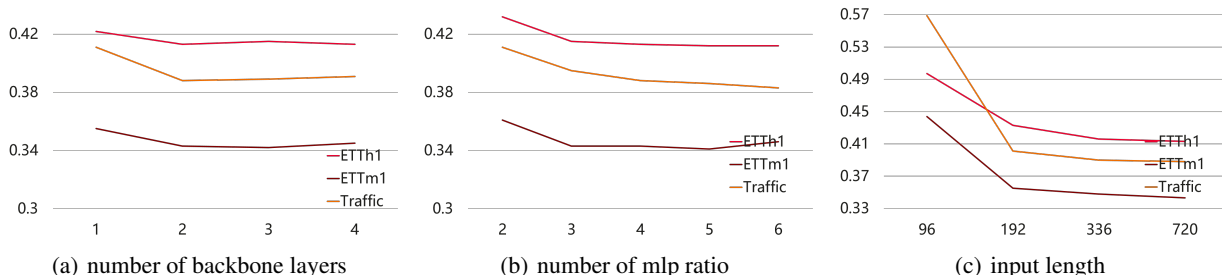
To verify our model’s robustness, we conduct noise injection experiments by adding Gaussian noise with $0.1 \times \mathcal{N}(0, 1)$ in the training/test stage. The results in Table 16 show that adding noise has a limited effect on our model’s performance, the deterioration is less than 1% in the worst case. Thanks to the introducing of the sparse operation on the un-salient part in the frequency domain, the model’s robustness is consistent across various tasks. Moreover, as shown in the last line, adding noise even on the train or test stage has no effect on the MSL dataset.

E. Parameter Sensitivity Analysis

E.1. Hyper-parameter sensitivity analysis

We conduct a hyperparameter sensitivity analysis focusing on the important hyper-parameters within ODFL: namely, the number of backbone model layers, the mlp ratio, the time series input length T . The correlated results can be found in Figure 7. We can find that our proposed ODFL can present a stable performance under different choices of hyper-parameters. And it shows that the performance first increases and then slightly decreases with respect to the increase of the model size because a large size improves the fitting ability of our ODFL but may easily lead to overfitting especially when the model is too large. Besides, the model can capture more temporal information with longer input sequence.

Figure 7. Analysis of hyper-parameter sensitivity.



E.2. Experiment error bar under different seeds

All experiments have been conducted three times with different seeds, and we present the standard deviations of our model. In Table 17, the average MSE and MAE have been reported across four ETT datasets, complete with standard deviations. The result shows that random seeds make very little impact on the ODFL.

Table 17. Standard deviations of our ODFL.

Dataset	ETTm1		ETTm2		ETTTh1		ETTTh2	
Metric	MSE	MAE	MSE	MAE	MSE	MAE	MSE	MAE
Result	0.343 ± 0.005	0.378 ± 0.003	0.246 ± 0.001	0.313 ± 0.004	0.413 ± 0.006	0.432 ± 0.008	0.331 ± 0.003	0.384 ± 0.001

F. Visualization

We provide the visualization of our learned kernel in the frequency domain on ETTTh1 dataset in Figure 8. The visualization shows that our kernel learns diversified and preferential frequency bands. Also, some of our kernels has learned the decaying structure introduced by SGConv (Li et al., 2022).

G. Full results

Due to the space limitation of the main text, we place the full results of all experiments in the following: long-term forecasting in Table 18, imputation in Table 20, short-term forecasting in Table 19, anomaly detection in Table 21, and classification in Table 22.

Table 18. Full results for the long-term forecasting task.

Models	ODFL (Ours)	TimesNet (2023)	ETS. (2022)	LightTS (2022)	DLinear (2023)	FED. (2022)	PatchTST (2023)	OFA (2023)	Cross. (2023)	SCINet (2022)	MICN (2023)	FreTS (2023)	
Metric	MSE MAE	MSE MAE	MSE MAE	MSE MAE	MSE MAE	MSE MAE	MSE MAE	MSE MAE	MSE MAE	MSE MAE	MSE MAE	MSE MAE	
ETTm1	96	0.282 <u>0.343</u>	0.338 0.375	0.375 0.398	0.374 0.400	0.299 0.343	0.379 0.419	<u>0.290</u> 0.342	0.292 0.346	0.316 0.373	0.325 0.372	0.314 0.360	0.301 0.348
	192	0.322 <u>0.368</u>	0.374 0.387	0.408 0.410	0.400 0.407	0.335 0.365	0.426 0.441	<u>0.332</u> 0.369	<u>0.332</u> 0.372	0.377 0.411	0.354 0.386	0.359 0.387	0.340 0.374
	336	0.356 <u>0.388</u>	0.410 0.411	0.435 0.428	0.438 0.438	0.369 0.386	0.445 0.459	<u>0.366</u> 0.392	<u>0.366</u> 0.394	0.431 0.442	0.394 0.415	0.398 0.413	0.373 0.397
	720	0.412 0.411	0.478 0.450	0.499 0.462	0.527 0.502	0.425 0.421	0.543 0.450	<u>0.416</u> <u>0.420</u>	0.417 0.421	0.600 0.547	0.476 0.469	0.459 0.464	0.433 0.425
ETTm2	96	0.160 0.253	0.187 0.267	0.189 0.280	0.209 0.308	0.167 0.260	0.203 0.287	<u>0.165</u> <u>0.255</u>	0.173 0.262	0.421 0.461	0.186 0.281	0.178 0.273	0.180 0.273
	192	0.214 0.290	0.249 0.309	0.253 0.319	0.311 0.382	0.224 0.303	0.269 0.328	<u>0.220</u> <u>0.292</u>	0.229 0.301	0.503 0.519	0.277 0.356	0.245 0.316	0.238 0.311
	336	0.267 0.328	0.321 0.351	0.314 0.357	0.442 0.466	0.281 0.342	0.325 0.366	<u>0.274</u> <u>0.329</u>	0.286 0.341	0.611 0.580	0.311 0.369	0.295 0.350	0.291 0.344
	720	0.344 0.380	0.408 0.403	0.414 0.413	0.675 0.587	0.397 0.421	0.421 0.415	<u>0.362</u> <u>0.385</u>	0.378 0.401	0.996 0.750	0.403 0.412	0.389 0.406	0.387 0.412
ETTth1	96	0.369 <u>0.402</u>	<u>0.384</u> <u>0.402</u>	0.494 0.479	0.424 0.432	0.375 0.399	0.376 0.419	<u>0.370</u> 0.400	0.376 0.391	0.386 0.429	0.375 0.406	0.396 0.427	0.373 0.409
	192	<u>0.409</u> 0.425	0.436 0.429	0.538 0.504	0.475 0.462	0.405 0.413	0.429 0.448	0.414 0.421	0.416 <u>0.418</u>	0.419 0.444	0.416 0.421	0.430 0.453	0.420 0.433
	336	<u>0.425</u> 0.441	0.491 0.469	0.574 0.521	0.518 0.488	0.439 0.443	0.459 0.465	0.422 0.440	0.442 0.433	0.440 0.461	0.504 0.495	0.433 0.458	0.438 0.441
	720	<u>0.449</u> <u>0.461</u>	0.521 0.500	0.562 0.535	0.547 0.533	0.472 0.490	0.506 0.507	0.447 0.468	0.477 0.456	0.519 0.524	0.544 0.527	0.474 0.508	0.473 0.510
ETTth2	96	0.269 0.335	0.340 0.374	0.340 0.391	0.397 0.437	0.289 0.353	0.358 0.397	<u>0.274</u> <u>0.336</u>	0.285 0.342	0.628 0.563	0.295 0.361	0.289 0.357	0.288 0.351
	192	0.330 <u>0.380</u>	0.402 0.414	0.430 0.439	0.520 0.504	0.383 0.418	0.429 0.439	<u>0.339</u> 0.379	0.354 0.389	0.703 0.624	0.349 0.383	0.409 0.438	0.380 0.413
	336	<u>0.331</u> <u>0.388</u>	0.452 0.452	0.485 0.479	0.626 0.559	0.448 0.465	0.496 0.487	0.329 0.384	0.373 0.407	0.827 0.675	0.365 0.409	0.417 0.452	0.449 0.462
	720	<u>0.391</u> <u>0.434</u>	0.462 0.468	0.500 0.497	0.863 0.672	0.605 0.551	0.463 0.474	0.379 0.422	0.406 0.441	1.181 0.840	0.475 0.488	0.426 0.473	0.536 0.515
Electricity	96	0.128 <u>0.224</u>	0.168 0.272	0.187 0.304	0.207 0.307	0.140 0.237	0.193 0.308	<u>0.129</u> 0.222	0.139 0.238	0.156 0.255	0.168 0.253	0.159 0.267	0.133 0.230
	192	0.145 0.240	0.184 0.289	0.199 0.315	0.213 0.316	0.153 0.249	0.201 0.315	<u>0.147</u> 0.240	0.153 0.251	0.231 0.309	0.175 0.262	0.168 0.279	0.152 0.251
	336	0.162 <u>0.260</u>	0.198 0.300	0.212 0.329	0.230 0.333	0.169 0.267	0.214 0.329	<u>0.163</u> 0.259	0.169 0.266	0.323 0.369	0.189 0.278	0.196 0.308	<u>0.163</u> <u>0.260</u>
	720	0.195 0.288	0.220 0.320	0.233 0.345	0.265 0.360	0.203 0.301	0.246 0.355	<u>0.197</u> <u>0.290</u>	0.206 0.297	0.404 0.423	0.231 0.316	0.203 0.312	0.209 0.316
Traffic	96	0.358 <u>0.251</u>	0.593 0.321	0.607 0.392	0.615 0.391	0.410 0.282	0.587 0.366	<u>0.360</u> 0.249	0.388 0.282	0.491 0.274	0.613 0.395	0.508 0.301	0.399 0.278
	192	0.374 0.254	0.617 0.336	0.621 0.399	0.601 0.382	0.423 0.287	0.604 0.373	<u>0.379</u> <u>0.256</u>	0.407 0.290	0.519 0.295	0.535 0.355	0.536 0.315	0.420 0.281
	336	0.386 0.264	0.629 0.336	0.622 0.396	0.613 0.386	0.436 0.296	0.621 0.383	<u>0.392</u> 0.264	0.412 0.294	0.513 0.289	0.540 0.358	0.525 0.310	0.422 0.301
	720	<u>0.433</u> <u>0.290</u>	0.640 0.350	0.632 0.396	0.658 0.407	0.466 0.315	0.626 0.382	0.432 0.286	0.450 0.312	0.530 0.300	0.620 0.394	0.571 0.323	0.453 0.308
Weather	96	0.145 0.198	0.172 0.220	0.197 0.281	0.182 0.242	0.176 0.237	0.217 0.296	<u>0.149</u> 0.198	0.162 0.212	0.153 0.217	0.178 0.233	0.161 0.226	0.163 0.216
	192	0.190 0.238	0.219 0.261	0.237 0.312	0.227 0.287	0.220 0.282	0.276 0.336	<u>0.194</u> <u>0.241</u>	0.204 0.248	0.197 0.269	0.235 0.277	0.220 0.283	0.200 0.262
	336	0.240 0.279	0.280 0.306	0.298 0.353	0.282 0.334	0.265 0.319	0.339 0.380	<u>0.245</u> <u>0.282</u>	0.254 0.286	0.252 0.311	0.337 0.345	0.275 0.328	0.247 0.285
	720	0.309 0.330	0.365 0.359	0.352 0.288	0.352 0.386	0.323 0.362	0.403 0.428	<u>0.314</u> <u>0.334</u>	0.326 0.337	0.318 0.363	0.396 0.413	<u>0.311</u> 0.356	0.318 0.342
ILL	24	1.301 0.748	2.317 0.934	2.527 1.020	8.313 2.144	2.215 1.081	3.228 1.260	<u>1.319</u> 0.754	2.063 0.881	3.040 1.186	2.150 1.005	2.684 1.112	2.127 1.062
	36	1.422 0.829	1.972 0.920	2.615 1.007	6.631 1.902	1.963 0.963	2.679 1.080	<u>1.430</u> 0.834	1.868 0.892	3.356 1.230	2.103 0.983	2.507 1.013	1.952 0.963
	48	1.539 0.807	2.238 0.940	2.359 0.972	7.299 1.982	2.130 1.024	2.622 1.078	<u>1.553</u> 0.815	1.790 0.884	3.441 1.223	2.432 1.061	2.423 1.012	1.832 0.891
	60	1.461 0.783	2.027 0.928	2.487 1.016	7.283 1.985	2.368 1.096	2.857 1.157	<u>1.470</u> <u>0.788</u>	1.979 0.957	3.608 1.302	2.325 1.035	2.653 1.085	1.992 0.971

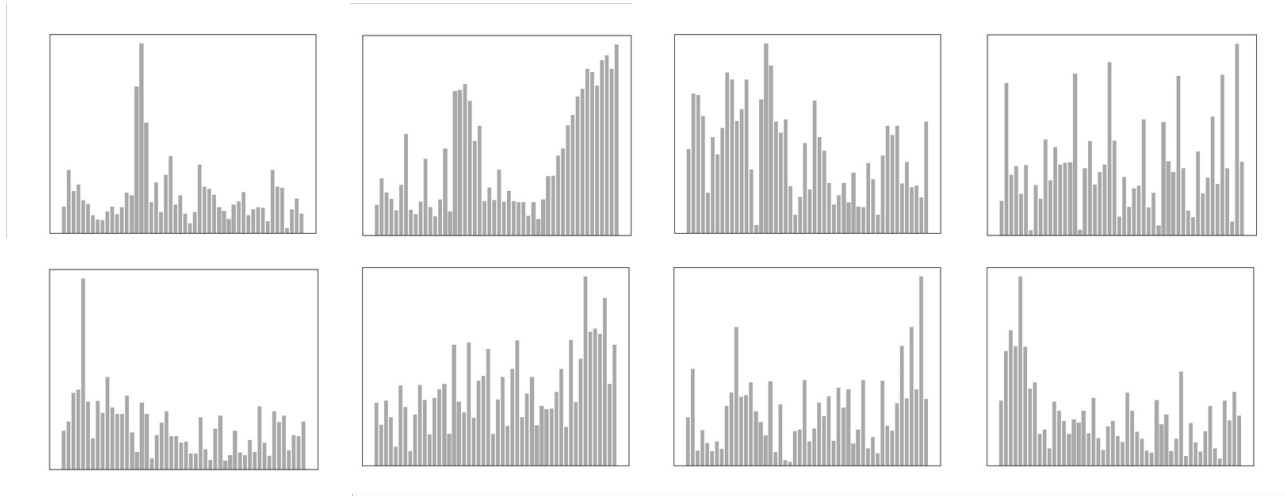


Figure 8. Visualization of our learned kernel. The horizontal axis represents index, the vertical axis represents the amplitude value of the kernel K .

Table 19. Full results for the short-term forecasting task.

Models		ODFL (Ours)	TimesNet (2023)	N-HiTS (2022)	N-BEATS (2019)	ETS (2022)	LightTS (2022)	DLinear (2023)	FED. (2022)	Stationary (2022)	Cross. (2023)	PatchTST (2023)	MICN (2023)	SCINet (2023)	OFA (2023)	FreTS (2023)
Yearly	SMAPE	13.235	<u>13.387</u>	13.418	13.436	18.009	14.247	16.965	13.728	13.717	13.392	13.477	14.935	13.717	13.531	13.448
	MASE	2.971	<u>2.996</u>	3.045	3.043	4.487	3.109	4.283	3.048	3.078	3.001	3.019	3.523	3.076	3.015	3.030
	OWA	0.779	<u>0.786</u>	0.793	0.794	1.115	0.827	1.058	0.803	0.807	0.787	0.792	0.900	0.807	0.793	0.793
Quarterly	SMAPE	9.993	<u>10.100</u>	10.202	10.124	13.376	11.364	12.145	10.792	10.958	16.317	10.380	11.452	10.845	10.177	10.127
	MASE	1.168	1.182	1.194	<u>1.169</u>	1.906	1.328	1.520	1.283	1.325	2.197	1.233	1.389	1.295	1.194	1.170
	OWA	0.880	0.890	0.899	<u>0.886</u>	1.302	1.000	1.106	0.958	0.981	1.542	0.921	1.026	0.965	0.898	<u>0.886</u>
Monthly	SMAPE	12.599	<u>12.670</u>	12.791	12.677	14.588	14.014	13.514	14.260	13.917	12.924	12.959	13.773	13.208	12.894	12.746
	MASE	0.926	<u>0.933</u>	0.969	0.937	1.368	1.053	1.037	1.102	1.097	0.966	0.970	1.076	0.999	0.956	0.943
	OWA	0.872	<u>0.878</u>	0.899	0.880	1.149	0.981	0.956	1.012	0.998	0.902	0.905	0.983	0.928	0.897	0.885
Others	SMAPE	4.885	<u>4.891</u>	5.061	4.925	7.267	15.880	6.709	4.954	6.302	5.493	4.952	6.716	5.423	4.940	5.264
	MASE	3.359	3.302	3.216	3.391	5.240	11.434	4.953	3.264	4.064	3.690	3.347	4.717	3.583	<u>3.228</u>	3.498
	OWA	1.044	<u>1.035</u>	1.040	1.053	1.591	3.474	1.487	1.036	1.304	1.160	1.049	1.451	1.136	1.029	1.105
Weighted Average	SMAPE	11.734	<u>11.829</u>	11.927	11.851	14.718	13.525	13.639	12.840	12.780	13.474	12.059	13.130	12.369	11.991	11.905
	MASE	1.576	<u>1.585</u>	1.613	1.599	2.408	2.111	2.095	1.701	1.756	1.866	1.623	1.896	1.677	1.600	1.605
	OWA	0.845	<u>0.851</u>	0.861	0.855	1.172	1.051	1.051	0.918	0.930	0.985	0.869	0.980	0.894	0.861	0.858

Table 20. Full results for the imputation task.

Models	ODFL	TimesNet	ETS.	LightTS	DLinear	FED.	PatchTST	Cross.	MICN	SCINet	OFA	FreTS	
	(Ours)	(2023)	(2022)	(2022)	(2023)	(2022)	(2023)	(2023)	(2023)	(2022)	(2023)	(2023)	
Ratio	MSE MAE	MSE MAE	MSE MAE	MSE MAE	MSE MAE	MSE MAE	MSE MAE	MSE MAE	MSE MAE	MSE MAE	MSE MAE	MSE MAE	
ETTm1	12.5%	0.011 0.076	0.019 0.092	0.067 0.188	0.075 0.180	0.058 0.162	0.035 0.135	0.041 0.128	0.037 0.137	0.039 0.137	0.031 0.116	<u>0.017 0.085</u>	0.027 0.115
	25%	0.014 0.083	0.023 0.101	0.096 0.229	0.093 0.206	0.080 0.193	0.052 0.166	0.043 0.130	0.038 0.141	0.059 0.170	0.036 0.124	<u>0.022 0.096</u>	0.035 0.122
	37.5%	0.017 0.090	<u>0.029 0.111</u>	0.133 0.271	0.113 0.231	0.103 0.219	0.069 0.191	0.044 0.133	0.041 0.142	0.080 0.199	0.041 0.134	<u>0.029 0.111</u>	0.038 0.130
	50%	0.022 0.099	<u>0.036 0.124</u>	0.186 0.323	0.134 0.255	0.132 0.248	0.089 0.218	0.050 0.142	0.047 0.152	0.103 0.221	0.049 0.143	0.040 0.128	0.043 0.139
ETTm2	12.5%	0.015 0.074	0.018 0.080	0.108 0.239	0.034 0.127	0.062 0.166	0.056 0.199	0.025 0.092	0.044 0.148	0.060 0.165	0.023 0.093	<u>0.017 0.076</u>	0.024 0.097
	25%	0.016 0.079	<u>0.020 0.085</u>	0.164 0.294	0.042 0.143	0.085 0.196	0.080 0.195	0.027 0.095	0.047 0.151	0.100 0.216	0.026 0.100	<u>0.020 0.080</u>	0.025 0.098
	37.5%	0.019 0.084	0.023 0.091	0.237 0.356	0.051 0.159	0.106 0.222	0.110 0.231	0.029 0.099	0.044 0.145	0.163 0.273	0.028 0.105	<u>0.022 0.087</u>	0.030 0.104
	50%	0.022 0.093	0.026 0.098	0.323 0.421	0.059 0.174	0.131 0.247	0.156 0.276	0.032 0.106	0.047 0.150	0.254 0.342	0.031 0.111	<u>0.025 0.095</u>	0.040 0.117
ETTth1	12.5%	0.027 0.115	0.057 0.159	0.126 0.263	0.240 0.345	0.151 0.267	0.070 0.190	0.094 0.199	0.099 0.218	0.072 0.192	0.089 0.202	<u>0.043 0.140</u>	0.082 0.198
	25%	0.040 0.139	0.069 0.178	0.169 0.304	0.265 0.364	0.180 0.292	0.106 0.236	0.119 0.225	0.125 0.243	0.105 0.232	0.099 0.211	<u>0.054 0.156</u>	0.089 0.203
	37.5%	0.055 0.159	0.084 0.196	0.220 0.347	0.296 0.382	0.215 0.318	0.124 0.258	0.145 0.248	0.146 0.263	0.139 0.267	0.107 0.218	<u>0.072 0.180</u>	0.102 0.209
	50%	0.069 0.178	<u>0.102 0.215</u>	0.293 0.402	0.334 0.404	0.257 0.347	0.165 0.299	0.173 0.271	0.158 0.281	0.185 0.310	0.120 0.231	0.107 0.216	0.115 0.230
ETTth2	12.5%	0.029 0.110	0.040 0.130	0.187 0.319	0.101 0.231	0.100 0.216	0.095 0.212	0.057 0.150	0.103 0.220	0.106 0.223	0.061 0.161	<u>0.039 0.125</u>	0.052 0.148
	25%	0.034 0.120	0.046 0.141	0.279 0.390	0.115 0.246	0.127 0.247	0.137 0.258	0.062 0.158	0.110 0.229	0.151 0.271	0.062 0.162	<u>0.044 0.135</u>	0.064 0.155
	37.5%	0.041 0.129	0.052 0.151	0.400 0.465	0.126 0.257	0.158 0.276	0.187 0.304	0.068 0.168	0.129 0.246	0.229 0.332	0.065 0.166	<u>0.051 0.147</u>	0.071 0.177
	50%	0.046 0.142	0.060 0.162	0.602 0.572	0.136 0.268	0.183 0.299	0.232 0.341	0.076 0.179	0.148 0.265	0.334 0.403	0.069 0.172	<u>0.059 0.158</u>	0.079 0.183
Electricity	12.5%	0.065 0.179	0.085 0.202	0.196 0.321	0.102 0.229	0.092 0.214	0.107 0.237	0.073 0.188	<u>0.068 0.181</u>	0.090 0.216	0.073 0.185	0.080 0.194	0.084 0.205
	25%	0.073 0.192	0.089 0.206	0.207 0.332	0.121 0.252	0.118 0.247	0.120 0.251	0.082 0.200	<u>0.079 0.198</u>	0.108 0.236	0.081 <u>0.198</u>	0.087 0.203	0.099 0.217
	37.5%	0.084 0.200	0.094 0.213	0.219 0.344	0.141 0.273	0.144 0.276	0.136 0.266	0.097 0.217	<u>0.087 0.203</u>	0.128 0.257	0.090 0.207	0.094 0.211	0.104 0.222
	50%	0.095 0.210	0.100 0.221	0.235 0.357	0.160 0.293	0.175 0.305	0.158 0.284	0.110 0.232	<u>0.096 0.212</u>	0.151 0.278	0.099 0.214	0.101 0.220	0.109 0.227
Weather	12.5%	0.020 0.040	<u>0.025 0.045</u>	0.057 0.141	0.047 0.101	0.039 0.084	0.041 0.107	0.029 0.049	0.036 0.092	0.036 0.088	0.028 0.047	0.026 0.049	0.036 0.083
	25%	0.024 0.045	0.029 0.052	0.065 0.155	0.052 0.111	0.048 0.103	0.064 0.163	0.031 0.053	0.035 0.088	0.047 0.115	0.029 <u>0.050</u>	<u>0.028 0.052</u>	0.042 0.111
	37.5%	0.025 0.049	<u>0.031 0.057</u>	0.081 0.180	0.058 0.121	0.057 0.117	0.107 0.229	0.034 0.058	0.035 0.088	0.062 0.141	<u>0.031 0.055</u>	0.033 0.060	0.050 0.117
	50%	0.029 0.053	<u>0.034 0.062</u>	0.102 0.207	0.065 0.133	0.066 0.134	0.183 0.312	0.039 0.066	0.038 0.092	0.080 0.168	<u>0.034 0.059</u>	0.037 0.065	0.069 0.138

Table 21. Full results for the anomaly detection task. The P, R and F1 represent the precision, recall and F1-score (%) respectively. F1-score is the harmonic mean of precision and recall. A higher value of P, R and F1 indicates a better performance.

Datasets		SMD			MSL			SMAP			SWaT			PSM			Avg F1
Metrics		P	R	F1	P	R	F1	P	R	F1	P	R	F1	P	R	F1	(%)
Anomaly	(2021)	88.91	82.23	85.49	79.61	87.37	83.31	91.85	58.11	71.18	72.51	97.32	83.10	68.35	94.72	79.40	80.50
OFA	(2023)	88.89	84.98	<u>86.89</u>	82.00	82.91	82.45	90.60	60.95	<u>72.88</u>	92.20	96.34	94.23	98.62	95.68	97.13	86.72
FreTS	(2023)	87.09	80.08	83.44	89.62	75.19	81.77	89.65	54.06	67.45	91.00	79.87	85.08	99.15	86.55	92.42	82.03
DLinear	(2023)	83.62	71.52	77.10	84.34	85.42	84.88	92.32	55.41	69.26	80.91	95.30	87.52	98.28	89.26	93.55	82.46
ETSformer	(2022)	87.44	79.23	83.13	85.13	84.93	<u>85.03</u>	92.25	55.75	69.50	90.02	80.36	84.91	99.31	85.28	91.76	82.87
LightTS	(2022)	87.10	78.42	82.53	82.40	75.78	78.95	92.58	55.27	69.21	91.98	94.72	93.33	98.37	<u>95.97</u>	<u>97.15</u>	84.23
FEDformer	(2022)	87.95	82.39	85.08	77.14	80.07	78.57	90.47	58.10	70.76	90.17	96.42	93.19	97.31	97.16	97.23	84.97
TimesNet	(2023)	87.76	82.63	85.12	82.97	85.42	84.18	91.50	57.80	70.85	88.31	96.24	92.10	98.22	92.21	95.21	85.49
Crossformer	(2023)	83.06	76.61	79.70	84.68	83.71	84.19	92.04	55.37	69.14	88.49	93.48	90.92	97.16	89.73	93.30	83.45
PatchTST	(2023)	87.42	81.65	84.44	84.07	86.23	85.14	92.43	57.51	70.91	80.70	94.93	87.24	98.87	93.99	96.37	84.82
SCINet	(2023)	85.97	82.57	84.24	84.16	82.61	83.38	93.12	54.81	69.00	87.53	94.95	91.09	97.93	94.15	96.00	84.74
MICN	(2023)	88.45	83.47	85.89	83.02	83.67	83.34	90.65	61.42	73.23	91.87	95.08	93.45	98.40	88.69	93.29	85.84
ODFL	(Ours)	88.47	85.66	87.04	89.68	79.77	84.43	90.29	57.74	70.44	90.73	96.50	<u>93.53</u>	98.60	94.01	96.26	<u>86.34</u>

Table 22. Full results for the classification task. We report the classification accuracy (%) results.

Datasets	CNN			RNN			MLP			Transformers				Ours	
	MICN (2023)	Rocket (2020)	SCINet (2022)	TimesNet (2023)	LSTNet (2018)	S4 (2022)	DLinear (2023)	LightTS (2022)	FreTS (2023)	ETS (2022)	PatchTST (2023)	Cross. (2023)	FED. (2022)	OFA (2023)	ODFL (Ours)
EthanolConcentration	35.3	45.2	34.4	35.7	39.9	31.1	36.2	29.7	28.9	28.1	32.8	38.0	31.2	34.2	36.6
FaceDetection	65.2	64.7	68.9	68.6	65.7	66.7	68.0	67.5	64.0	66.3	68.3	68.7	66.0	69.2	69.5
Handwriting	25.5	58.8	23.6	32.1	25.8	24.6	27.0	26.1	25.6	32.5	29.6	28.8	28.0	32.7	32.7
Heartbeat	74.7	75.6	77.5	78.0	77.1	72.7	75.1	75.1	76.6	71.2	74.9	77.6	73.7	77.2	77.5
JapaneseVowels	94.6	96.2	96.0	98.4	98.1	98.4	96.2	96.2	93.2	95.9	97.5	99.1	98.4	98.6	98.6
PEMS-SF	85.5	75.1	83.8	89.6	86.7	86.1	75.1	88.4	87.3	86.0	89.3	85.9	80.9	87.9	87.5
SelfRegulationSCP1	86.0	90.8	92.5	91.8	84.0	90.8	87.3	89.4	90.8	89.6	90.7	92.1	88.7	93.2	93.2
SelfRegulationSCP2	53.6	53.3	57.2	57.2	52.8	52.2	50.5	51.1	55.6	55.0	57.8	58.3	54.4	59.4	58.0
SpokenArabicDigits	97.1	71.2	98.1	99.0	100.0	100.0	81.4	100.0	96.1	100.0	98.3	97.9	100.0	99.2	100.0
UWaveGestureLibrary	82.8	94.4	85.1	85.3	87.8	85.9	82.1	80.3	85.0	85.0	85.8	85.3	85.3	88.1	87.2
Average Accuracy	70.0	70.9	71.7	73.6	71.8	70.9	67.5	70.4	70.3	71.0	72.5	73.2	70.7	<u>74.0</u>	74.1